Study on Azophotoswitches containing thiazole, isothiazole, thiadiazole and isothiadiazole

(チアゾール、イソチアゾール、チアジアゾール、イソチアジアゾールを含むアゾフォトスイッチに関する研究)

A Thesis

Submitted for the Degree of

Doctor of Philosophy

By

Madappuram Cheruthu Nusaiba

Division of Soft Matter Science

Graduate School of Life Science

Hokkaido University, Japan

2025/3

Contents

1. Introduction

Photoswitches are molecules that exist in two distinct isomeric forms, often referred as *cis* and *trans* configurations, in response to light irradiation. These forms differ in their spatial arrangement of atoms, resulting in unique physical and chemical properties. Photoswitchable motifs include a wide range of systems such as azobenzenes, spiropyrans, diarylethenes, arylhydrazones, fulgides/fulgimides, stilbenes, donor-acceptor Stenhouse adducts, and norbornadiene/quadricyclane derivatives[1,2] (Figure 1). When exposed to light of a certain wavelength, the molecule absorbs photons, which provide the energy needed to break or rearrange molecular bonds, leading to a change in the geometry of the molecule. This change alters properties such as shape, electronic distribution, or dipole moment, effectively converting the molecule from one isomeric form to another. For instance, under ultraviolet (UV) or visible light, azobenzene photoswitches may transition from a linear *trans* state to a more compact *cis* state, and this process is often reversible. By simply irradiating the molecule with a different wavelength of light, or keeping in dark, it can revert to its original isomeric form. This process of reversible switching between these isomers in response to light irradiation is known as photoisomerization. This reversible switching mechanism allows photoswitches to be used in various applications such as material and biological sciences, where dynamic control over molecular structure and function is required.[3,4]

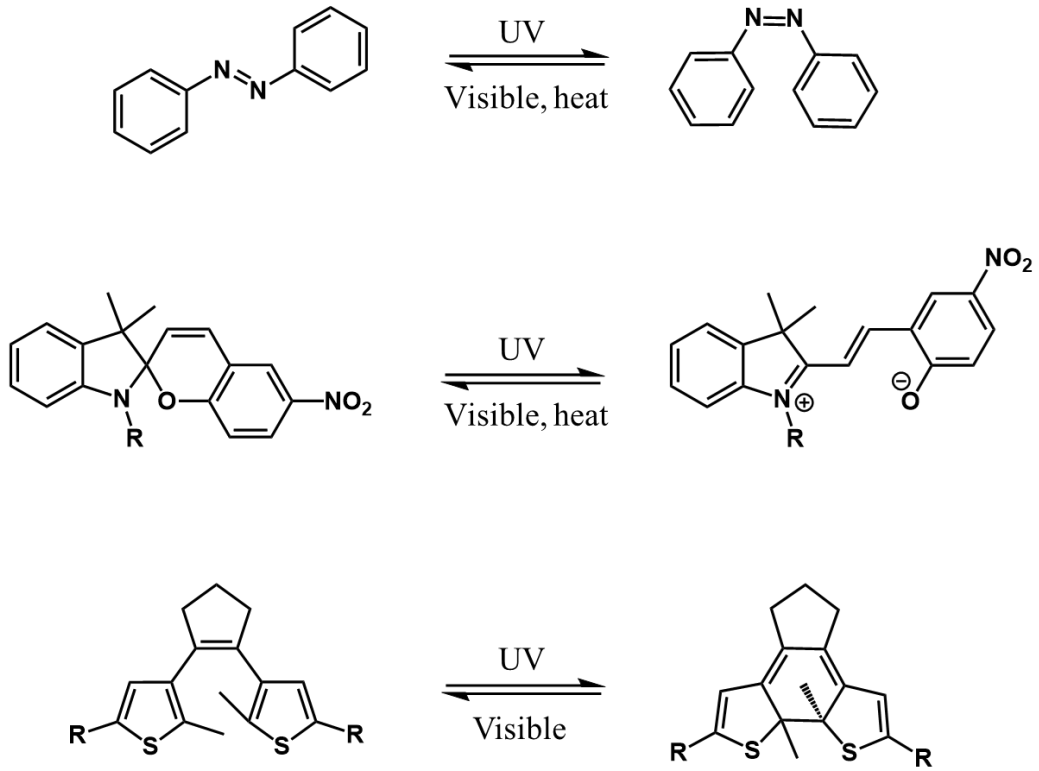

Figure 1: Structure of the photoswitches. Azobenzene (top), Spiropyran (middle left) and Diarylethene (bottom).

A photoswitch's performance can be evaluated by several key parameters, including the maximum wavelength of absorption, quantum yield, the relative thermal stability of the two isomers, the composition of isomers at equilibrium, and the reproducibility of photochemical switching. The maximum wavelength of absorption (λ_{max}) indicates the specific wavelength at which the molecule can efficiently absorb light, which is crucial for determining the optimal conditions for switching. Quantum yield measures the efficiency of the photoisomerization process, indicating how many molecules successfully convert from one isomer to another upon light exposure. The relative thermal stability of the two isomers (half-life) is also important, as

it determines how long each isomer can persist before reverting to its original state due to thermal energy. Additionally, the composition of isomers at equilibrium indicates the proportion of each isomer present under ambient conditions, while the reproducibility of photochemical switching assesses the consistency and reliability of the switching process over multiple cycles. Azobenzene is one of the well-studied photoswitches with the wavelength of maximum absorbance (λ_{max}) is at ~320 nm can switch from a planar *trans* configuration to a bent *cis* form when exposed to 365-nm UV light, and revert back to the *trans* form upon exposure to visible light or thermally in the dark (Figure 1, top). However, the reliance on UV light poses challenges its applications in biological system. One method to improve the performance of azobenzene photoswitches is the introduction of substituents at the aryl rings. For instance, the λ_{max} of azobenzene can be shifted to longer wavelengths by adding electron-donating groups such as amino (NH_2), methoxy (OMe), or N,N-dimethyl (NMe_2) to the phenyl ring. These modifications enable azobenzene derivatives to absorb in the visible region, but typically result in a decrease in the thermal stability of the *cis* isomer.[5,6,7] Sadovski et al.demonstrated that introducing ortho-amino-substituted azobenzene shifted the λ_{max} to approximately 450 nm, though the thermal half-life of the *cis* isomer was reduced to milli seconds (Figure 2a). Similarly, Beharry et al. showed that ortho methoxy substitution could achieve red-shifted absorption while also significantly prolonging the thermal half-life of the *cis* isomer, making these derivatives more suitable for applications requiring visible light activation and longer-lived isomers (Figure 2b).

(a)

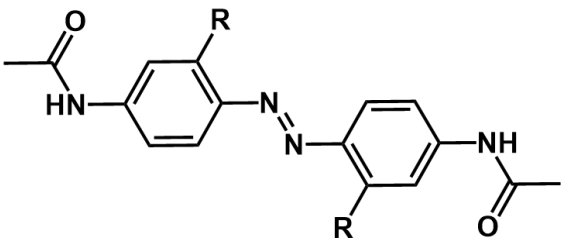

(1a-f)

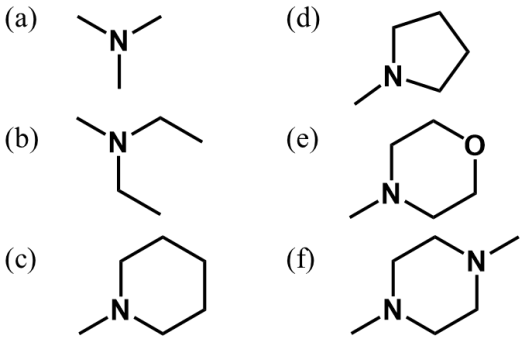

(b)

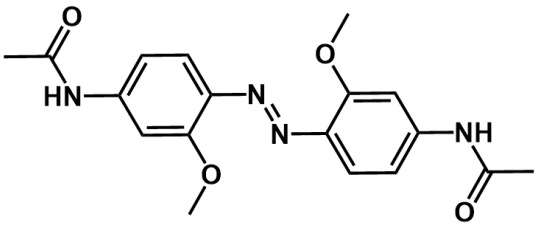

(2)

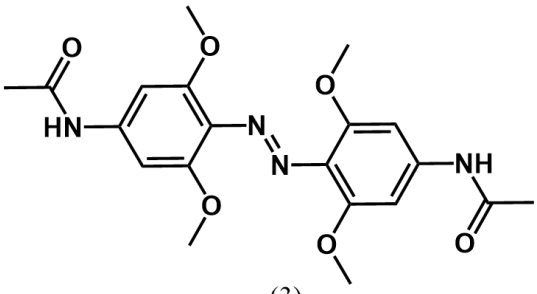

(3)

Figure 2: Molecular structure of substituted Azobenzene (a) series of *ortho*-amino substituted azobenzene derivatives, (b) *ortho*-methoxy substituted azobenzene derivatives.

Another approach to enhance the photophysical properties of azobenzene is the introduction of heteroaryl groups, which can further modify its absorption characteristics and switching behavior. Photoswitches containing "heteroaryl" units have garnered increasing attention due to their unique light absorption and photoisomerization properties.[8] These systems, which are characterized by their diverse electronic structures, exhibit distinct photophysical behaviors. 5-membered "heteroaryl" units have shown significant differences in both their photophysical and structural properties.[9] These variations are primarily attributed to the electronic and steric factors imparted by the heteroatoms within the ring. Several studies, including our own, have reported photoswitches incorporating five-membered heteroaryl units such as pyrrole, pyrazole, imidazole, isoxazole, triazole, thiazole, and thiophene. Each of these photoswitches displays photophysical properties that are largely influenced by the nature of the specific heteroaryl group present.[10, 11, 12, 13, 14, 15, 16, 17, 18, 19, 20] For example, phenylazopyrrole derivatives, which contain a pyrrole unit, require UV light for *trans–cis* isomerization (Figure 3).[21, 22] Despite this,

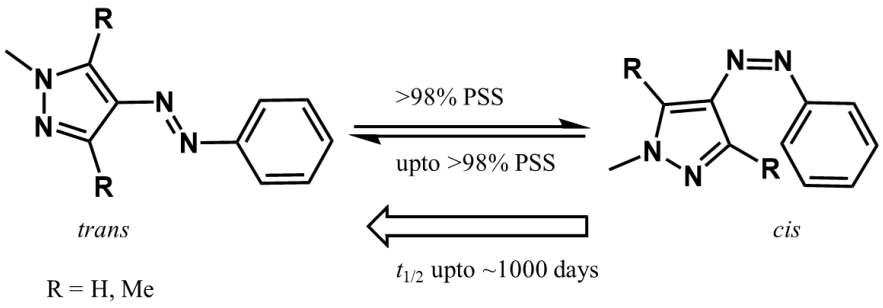

Figure 3: Molecular structures of phenylazopyrrol photoswitches and their isomerization

their *cis* isomers exhibit unusually long half-lives, indicating high stability in the photoisomerized state.

In a more recent study from our group, we explored the behavior of phenylazothiazole (PAT) photoswitches (Figure 4). These compounds demonstrate a significant red-shift in their absorption maxima. The *trans* isomer has a λ_{max} of 364 nm, which is 44 nm longer than the λ_{max} of azobenzene. This red-shift allows the phenylazothiazole derivatives to undergo *trans*-to-*cis* isomerization when irradiated with 405 nm light, which falls within the visible range.

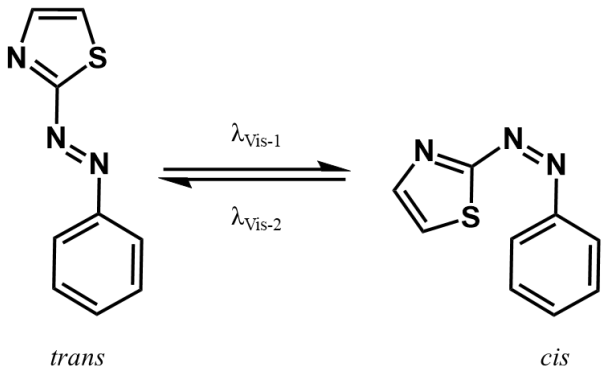

Figure 4: Molecular structures of phenylazothiazole photoswitches and their isomerization

This capability to isomerize under visible light is a major advantage, as it bypasses the need for harmful UV light. Furthermore, the reverse *cis*-to-*trans* isomerization can be induced by light at 525 nm, further expanding the usability of these compounds under longer-wavelength visible light. The ability to undergo photoisomerization using only visible light makes phenylazothiazoles more practical for applications where UV exposure is undesirable or

impractical (Figure 5). In addition to their visible-light responsiveness, the thermal stability of the *cis* isomers of phenylazothiazole photoswitches shows a moderate half-life of 2.8 hours in acetonitrile at 25°C, a decrease associated with the shift to visible light activation.

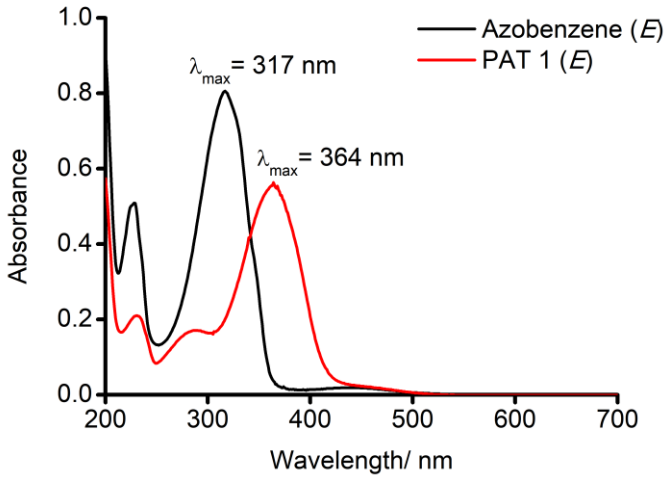

Figure 5: UV−visible absorption spectra of azobenzene and phenylazothiazole (PAT) in acetonitrile at 25 °C.

Many pharmacologically active compounds contain one or more units of five-membered heteroaryl groups[23, 24, 25, 26, 27] and their photoisomerizable forms can be useful for application in

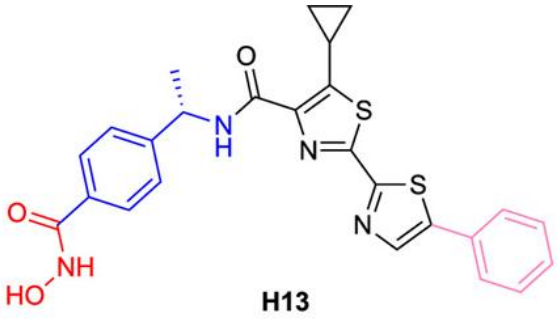

H13

Figure 6: Molecular structure of the bisthiazole-based compound H13

photopharmacology. For example, a bisthiazole-based compound, H13, shows potent inhibitory activity toward human histone deacetylases (HDACs) and exhibits significant anti-proliferative effects against various cancer cell lines (Figure 6). The development of new photoswitches is essential to enhance the versatility and efficiency of light-responsive molecules.

The purpose of this study is to explore how the five-membered heteroaryl groups influence the λ_{max} related to the isomerization wavelength of light and the thermal isomerization rates of the photoswitchable compounds. Heteroaryl groups, including oxazole, isothiazole, thiadiazole, and isothiadiazole, were chosen, which influence the electronic environment of the azo bond, thereby altering the absorption properties of the photoswitch. In this dissertation, I introduce a set of azo photoswitchable compounds containing these heteroaryl groups. One interesting finding was that incorporating both thiazole and isothiazole groups into the photoswitches shifted the λ_{max} to longer wavelengths compared to other compounds studied, though this was accompanied by a decrease in the *cis*-isomer lifetime, similar to trends observed in substituted azobenzenes. By designing photoswitches with absorption in the visible-light range, this study addresses one of the key challenges in photopharmacology: the need for biologically compatible activation wavelengths that minimize phototoxicity and tissue damage.

2. Experimental section

2.1 Chemicals

All reagents and solvents were purchased from commercial sources (FUJIFILM Wako Pure Chemical Corporation, Tokyo Chemical Industry, Merck, Kanto Chemical) and used without further purification. Reactions progress was monitored using thin-layer chromatography with TLC silica gel 60 F254 (Merck). Column chromatography was performed using silica gel 60 N (spherical, neutral, 40-50 μm, 63-210 μm, Kanto chemical).

2.2 General methods, instrumentation and measurements

NMR spectra (^{1}H, ^{13}C) were measured by a JEOL ECX-400 (400 or 600 MHz) spectrometer using tetramethylsilane as an internal standard. Electronspray ionization mass spectrometry (ESI) was performed on Thermo Scientific Exactive Plus.

A Shimadzu UV spectrophotometer (UV-1800) equipped with a TCC-100 Shimadzu temperature-controlled cell holder was used for recording the absorption spectra. Photoisomerization studies were carried out using a LED light source (Asahi Spectra, CL-1503) with LED heads emitting at 365 nm, 405 nm, 430 nm, 450 nm, 470 nm, 525 nm, and 568 nm.

The absorbance spectra of the fast-switching compounds **4** and **6** were acquired using an Agilent 8453 spectrophotometer under continuous irradiation at specific wavelengths. Each sample was irradiated unilaterally in the cuvette, and spectra were recorded during irradiation

once the photostationary state (PSS) was reached. For compound **4**, irradiation was maintained at 405 nm for *trans*-to-*cis* isomerization, followed by 525 nm for the *cis*-to-*trans* conversion. Similarly, compound **6** was continuously irradiated at 430 nm for *trans*-to-*cis* isomerization and at 568 nm for the *cis*-to-*trans* reversion while recording absorbance spectra.

2.3 Synthesis

In the study, I focused on the synthesis of eight compounds (**1**–**8**) using a streamlined, general one-step procedure (Figure 7)

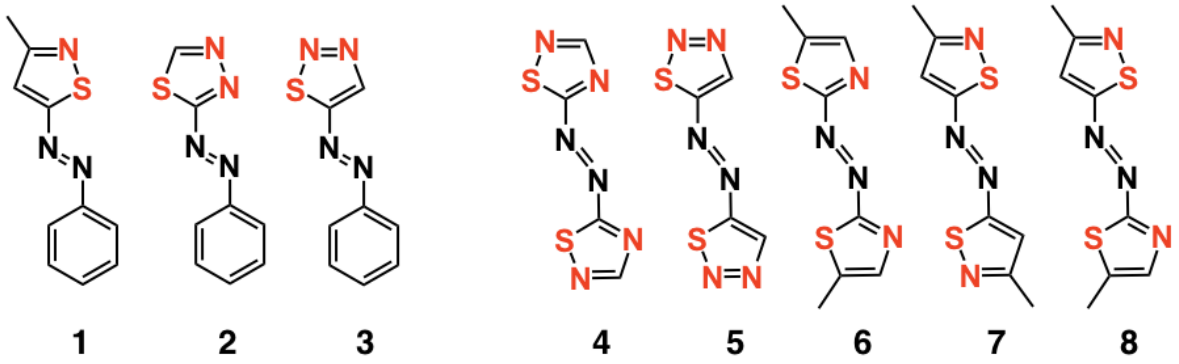

Figure 7: Molecular structures of synthesized compounds **1**–**8**.

For compounds **1**–**3**, I employed Mill's reaction, a well-established method for synthesizing azobenzenes, through the reaction of 2-amino heteroarene derivatives with nitrosobenzene. This reaction involves the formation of an azo bond between the aromatic units, which is crucial for

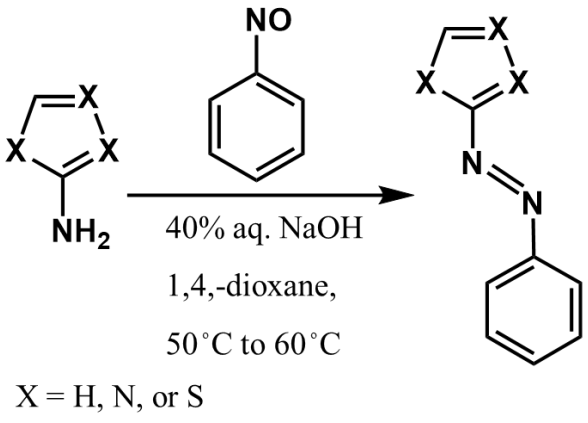

Scheme 1: General Synthetic scheme for compounds **1-3**.

generating photoswitchable compounds. While the standard Mill's reaction provides a foundation for this synthesis, I optimized the reaction conditions to improve yields and reaction times. This optimization included varying parameters such as temperature, solvent choice, and reaction time to achieve the desired products more efficiently. The specific reaction conditions employed for compounds **1**–**3** is detailed in Scheme 1.

For the synthesis of compounds **4**–**8**, I utilized methods based on oxidation, specifically focusing on the oxidation of the corresponding 2-amino heteroarene derivatives. (Scheme 2). For compounds **4**–**7**, I employed a method centered on homo-oxidation, which involves the oxidation of identical 2-amino heteroarene derivatives to generate azo compounds effectively. For the synthesis of the asymmetric heteroaryl azo compound **8**, the method involves the oxidation of two different 2-amino heteroarene derivatives. This strategy not only facilitates the formation of the azo bond but also introduces structural diversity into the compound, enhancing its potential

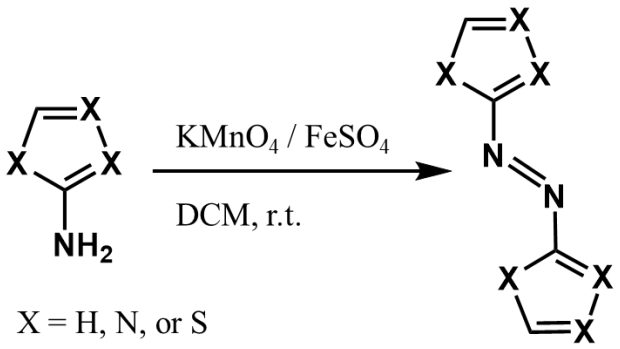

Scheme 2: General Synthetic scheme for compounds **4**-**8**.

photophysical properties. By utilizing these oxidation methods, I aimed to produce a range of azo compounds with distinct characteristics while simplifying the synthetic process.

Synthetic procedure of photoswitches

Compound **1**

To a warm (40 °C) NaOH solution (40% aq., 1 mL), 5-amino-3-methylisothiazole hydrochloride (2.3 mmol) in 1,4-dioxane (2.5 mL) was added and gently heated to 60 °C. Then, nitrosobenzene (2.53 mmol) was added slowly, and the mixture was stirred for 2 hours. The reaction mixture was then cooled and quenched with water and extracted with ethyl acetate (3 x 25 mL). The organic layer was washed with brine, dried over MgSO4, and concentrated in vacuo. The target compound was then isolated by column chromatography using a 2% ethyl acetate in hexane mixture, yielding an orange solid. (10.56%).

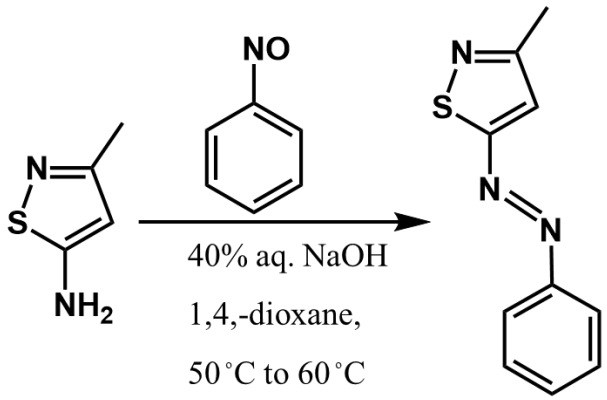

Scheme 3: Synthetic scheme for compound **1**.

^{1}H NMR (400 MHz, CDCl3) δ 7.89 (d, J = 9.6 Hz, 2H), 7.59 (s, 1H), 7.51 (m, 3H), 2.55 (s, 3H). ^{13}C NMR (400 MHz, CDCl3) δ 179.3, 167.4, 151.9, 132.6, 129.4, 125.0, 123.5, 19.8.

Compound **2**

To a warm (40 °C) NaOH solution (40% aq., 1 mL), 2-amino-1,3,4-thiadiazole (2.3 mmol) in 1,4-dioxane (2.5 mL) was added and gently heated to 60 °C. Then, nitrosobenzene (2.53 mmol) was added slowly, and the mixture was stirred for 2 hours. The reaction mixture was then cooled and quenched with water and extracted with ethyl acetate (3 x 25 mL). The organic layer was washed with brine, dried with MgSO4, and concentrated in vacuo followed by isolation of target compound by column chromatography using 20% ethyl acetate: hexane affording orange solid (14%).

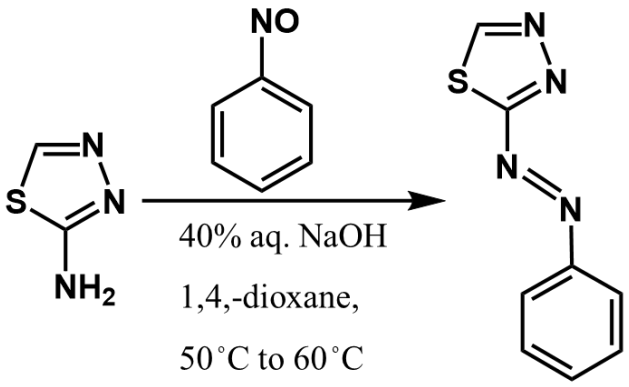

Scheme 4: Synthetic scheme for compound **2**.

^{1}H NMR (400 MHz, CDCl3) δ 9.14 (s, 1H), 8.11 (d, J = 12.5 Hz, 2H), 7.62 - 7.56 (m, 3H). ^{13}C NMR (400 MHz, CDCl3) δ 179.9, 153.0, 151.6, 134.3, 129.6, 124.4.

Compound **3**

To a warm (40 °C) NaOH solution (40% aq., 1 mL), 5-amino-1,2,3-thiadiazole (2.3 mmol) in 1,4-dioxane (2.5 mL) was added and gently heated to 60 °C. Then, nitrosobenzene (2.53 mmol) was added slowly, and the mixture was stirred for 2 hours. The reaction mixture was then cooled and quenched with water and extracted with ethyl acetate (3 x 25 mL). The organic layer was washed with brine, dried with MgSO4, and concentrated in vacuo followed by isolation of target compound by column chromatography using 60% dichloromethane: hexane affording orange solid (4.0%).

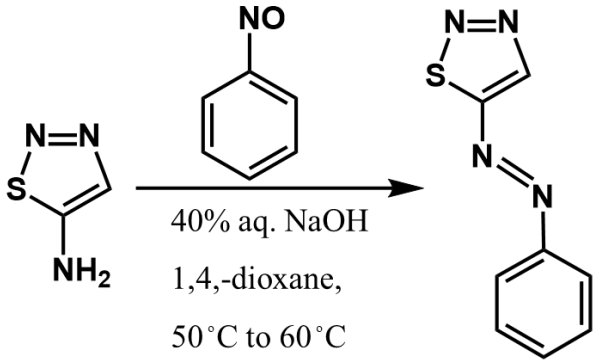

Scheme 5: Synthetic scheme for compound **3**.

^{1}H NMR (400 MHz, CDCl3) δ 9.24 (s, 1H), 7.95 (d, J = 12.3 Hz, 2H), 7.58 - 7.53 (m, 3H). ^{13}C-NMR (400 MHz, CDCl3) δ 171.0, 152.1, 146.6, 133.7, 129.5, 123.8.

Compound **4**

To cold sodium hypochlorite solution (15 mL), cool suspension of 5-amino-1,2,4-thiadiazole (2.9 mmol) in dichloromethane (10 mL) was added little by little followed by stirring for 1 hour at 0 °C. The reaction mixture was quenched with water and extracted with dichloromethane (3 x 25 mL). The organic layer was washed with brine, dried over MgSO4, and concentrated in vacuo. The target compound was isolated by column chromatography using ethyl acetate: hexane (10:90, v/v) as the eluent, yielding an orange solid (36.0%).

^{1}H NMR (400 MHz, CDCl3) δ 8.96 (s, 2H). ^{13}C-NMR (400 MHz, CDCl3) δ 192.2, 164.1.

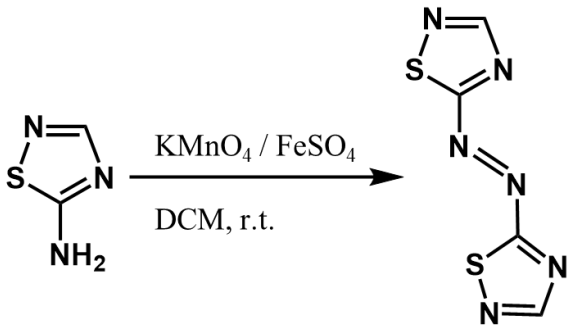

Scheme 6: Synthetic scheme for compound **4**.

Compound **5**

5-amino-1,2,3-thiadiazole (5 mmol) was dissolved in dichloromethane (50 mL). Potassium permanganate (15 mmol) and ferrous sulfate heptahydrate (10 mmol) were ground together until homogenous. The resulting powder was added to the dichloromethane solution. The mixture was stirred for 24 hours at room temperature. Afterward, the reaction mixture was filtered through celite, and the solvent evaporated. Finally, the target compound was isolated using column chromatography by 15% ethyl acetate: hexane affording orange red solid (4.6%).

^{1}H NMR (400 MHz, CDCl3) δ 9.29 (s, 2H). ^{13}C-NMR (400 MHz, CDCl3) δ 168.8, 148.5.

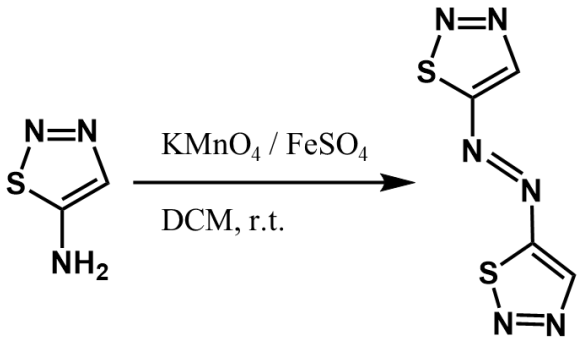

Scheme 7: Synthetic scheme for compound **5**.

Compound **6**

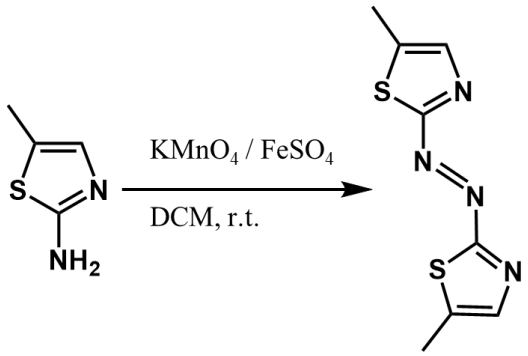

Scheme 8: Synthetic scheme for compound **6**.

2-amino-5-methylthiazole (4.38 mmol) was dissolved in dichloromethane (50 mL). Potassium permanganate (13.2 mmol) and ferrous sulfate heptahydrate (8.76 mmol) were ground together until homogenous. The resulting powder was added to the dichloromethane solution. The mixture was stirred for 24 hours at room temperature. Afterward, the reaction mixture was filtered through celite, and the solvent evaporated. Finally, the compound was isolated by column chromatography by 30% ethyl acetate: hexane affording orange red solid (18.3%).

^{1}H NMR (400 MHz, CDCl3) δ 7.78 (s, 1H), 2.56 (s, 3H). ^{13}C NMR (400 MHz, CDCl3) δ 173.3, 143.4, 139.9, 13.2.

Compound **7**

5-amino-3-methylisothiazole hydrochloride (3.3 mmol) was dissolved in dichloromethane (50 mL). Potassium permanganate (6.6 mmol) and ferrous sulfate heptahydrate (4.4 mmol) were ground together until homogenous. The resulting powder was added to the dichloromethane solution. The mixture was stirred for 24 hours at room temperature. Afterward, the reaction mixture was filtered through celite, and the solvent evaporated. Finally, the target compound was isolated using column chromatography by 2% ethyl acetate: hexane affording orange solid (35.5%).

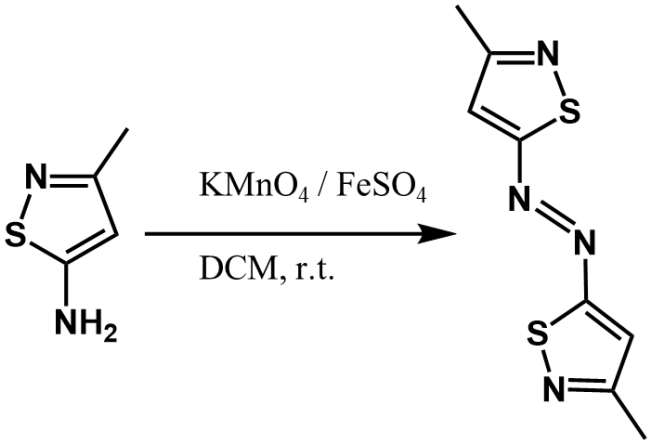

Scheme 9: Synthetic scheme for compound **7**.

^{1}H NMR (400 MHz, CDCl3) δ 7.58 (s, 1H), 2.54 (s, 3H). ^{13}C NMR (400 MHz, CDCl3) δ 177.7, 167.7, 126.5, 19.7.

Compound **8**

2-amino-5-methylthiazole (8.75 mmol) and 5-amino-3-methylisothiazole hydrochloride (8.75 mmol) was dissolved in dichloromethane. Potassium permanganate (26.25 mmol) and ferrous sulfate heptahydrate (17.5 mmol) were ground together until homogenous. The resulting powder was added to the dichloromethane solution. The mixture was stirred for 24 hours at room temperature. Afterward, the reaction mixture was filtered through celite, and the solvent evaporated. Finally, the target compound was isolated using column chromatography by 10% ethyl acetate: hexane affording orange red solid (7.3%).

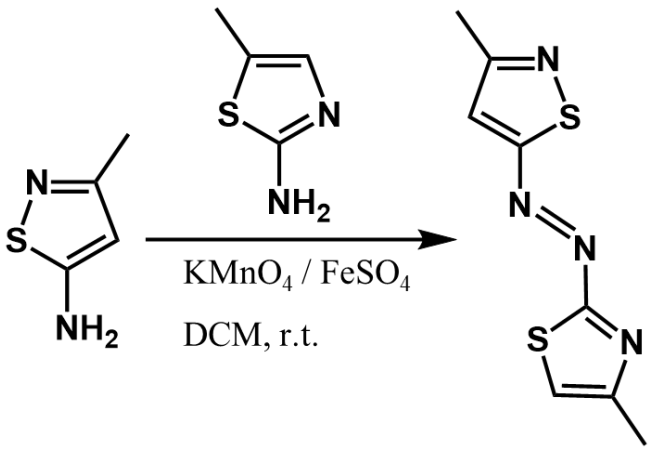

Scheme 10: Synthetic scheme for compound **8**.

^{1}H NMR (400 MHz, CDCl3) δ 7.77 (s, 1H), 7.61 (s, 1H), 2.57 (s, 3H), 2.55 (s, 3H). ^{13}C NMR (400 MHz, CDCl3) δ 177.5, 173.4, 167.4, 143.4, 139.8, 126.1, 19.7, 13.1.

2.4 NMR spectra (^{1}H, ^{13}C) and Mass spectra of compounds 1-8.

Compound **1**

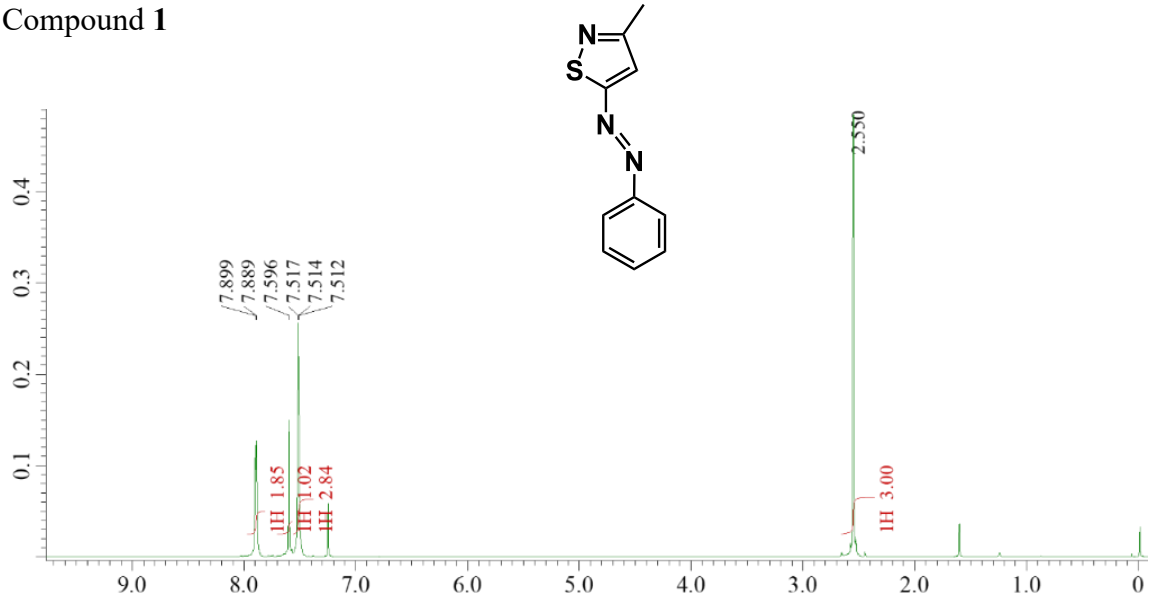

Figure 8: ^{1}H NMR of compound **1** in $CDCl_3$.

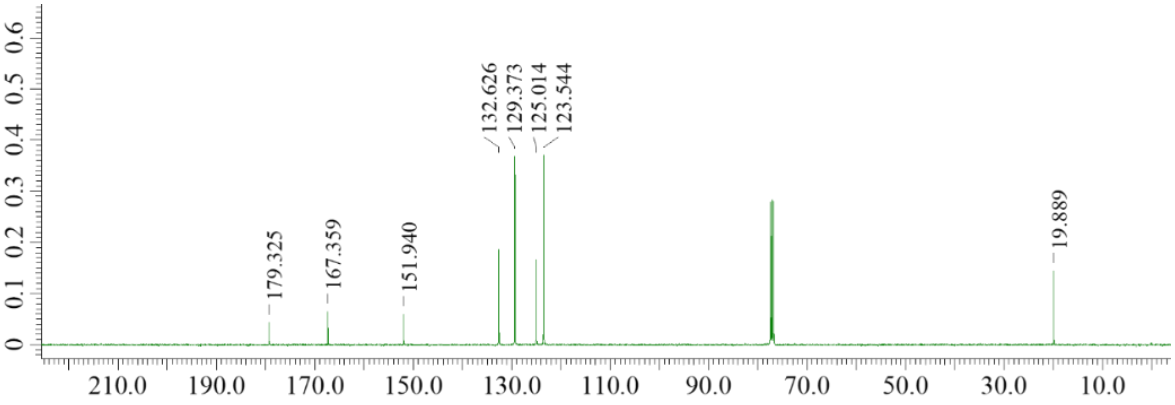

Figure 9: ^{13}C NMR of compound **1** in $CDCl_3$.

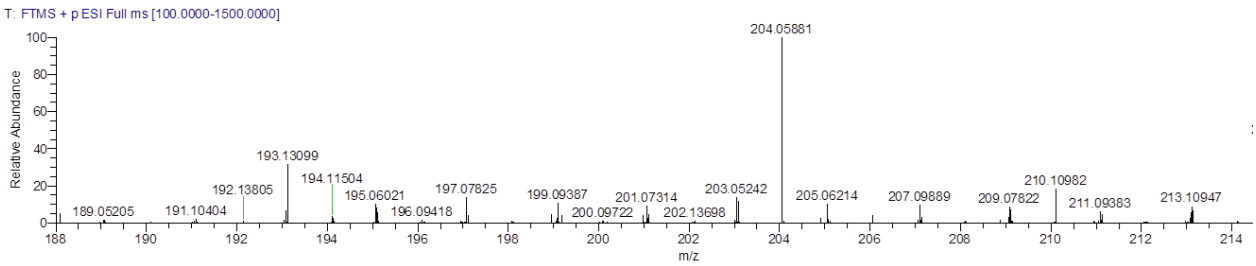

Figure 10: High-resolution mass spectra (ESI) of compound **1**. *m/z* $[M + H]^+$ calculated for $C_{10}H_9N_3S$: 204.06, found: 204.05

Compound **2**

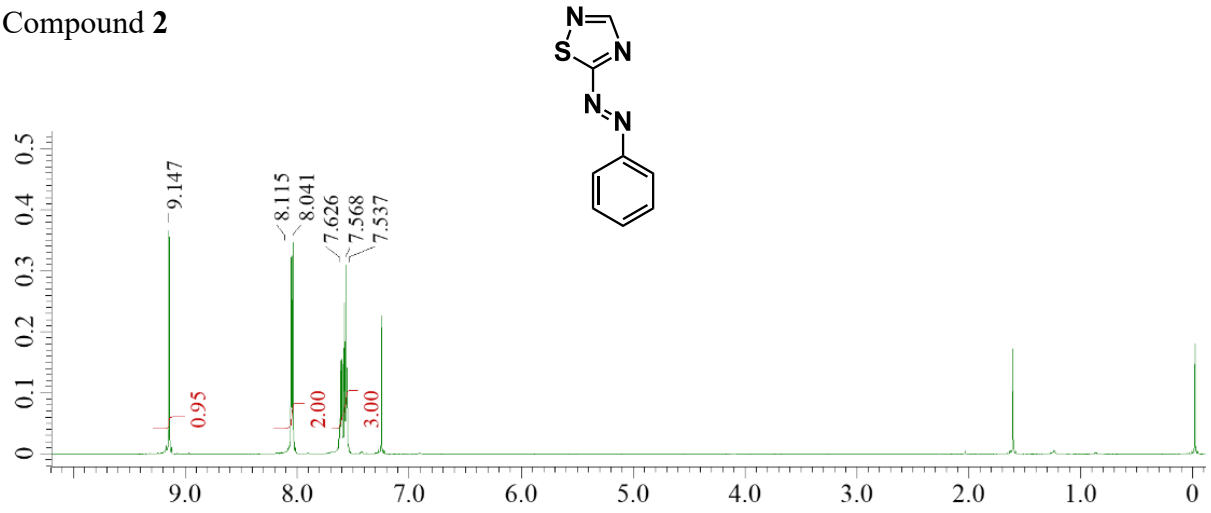

Figure 11: ^{1}H NMR of compound **2** in $CDCl_3$.

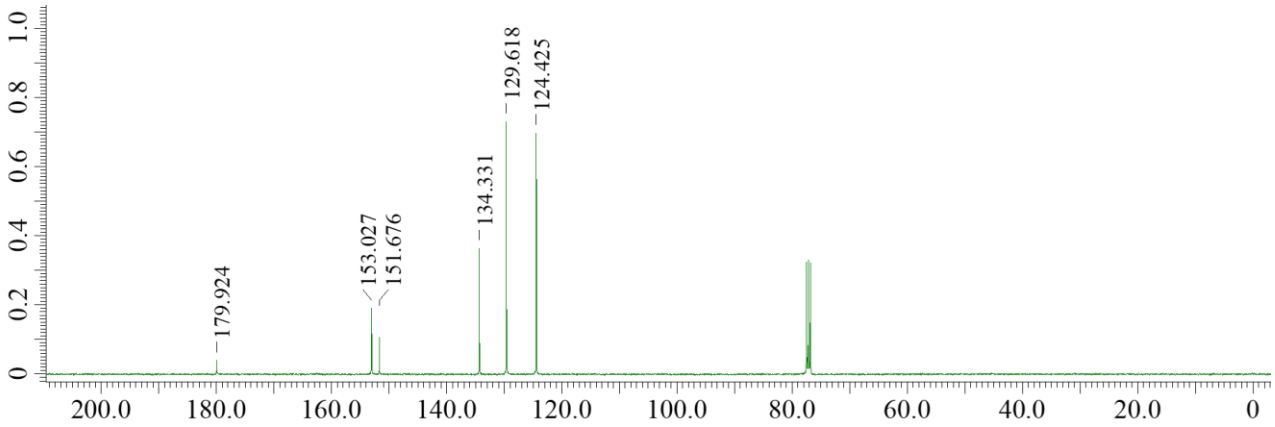

Figure 12: ^{13}C NMR of compound **2** in $CDCl_3$.

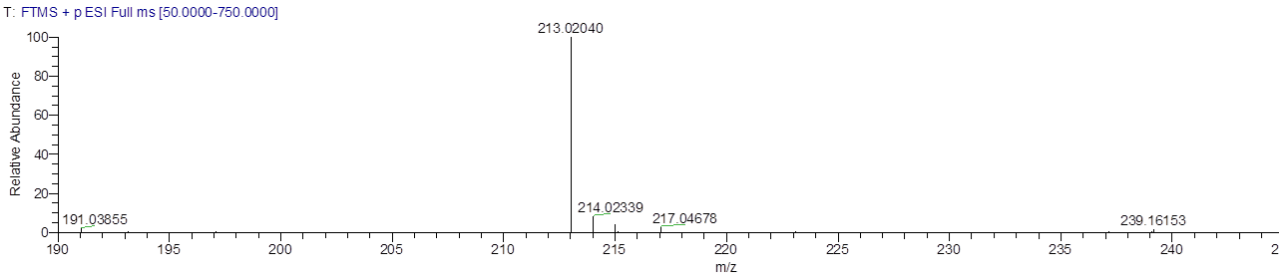

Figure 13: High-resolution mass spectra (ESI) of compound **2.** *m/z* $[M + Na]^+$ calculated for $C_8H_6N_4S$: 213.02, found: 213.02

Compound **3**

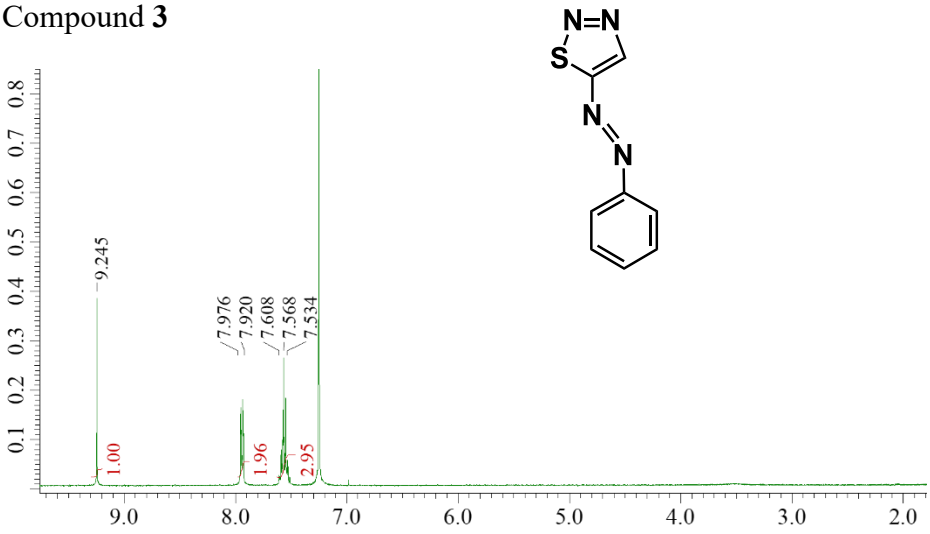

Figure 14: ^{1}H NMR of compound **3** in $CDCl_3$.

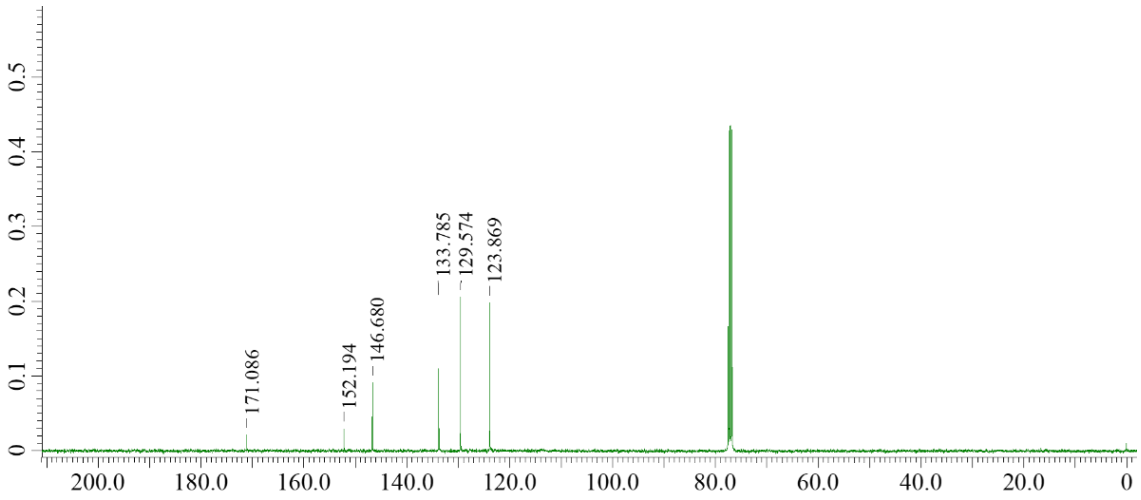

Figure 15: ^{13}C NMR of compound **3** in $CDCl_3$.

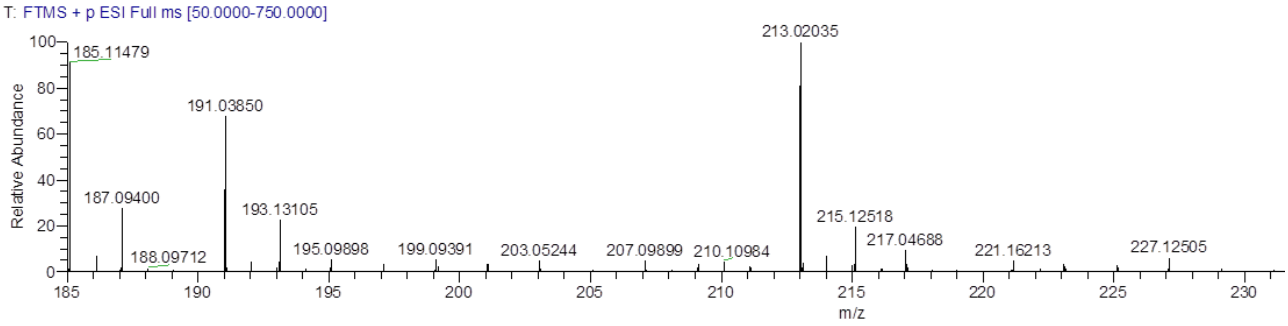

Figure 16: High-resolution mass spectra (ESI) of compound **3.** *m/z* $[M + Na]^+$ calculated for $C_8H_6N_4S$: 213.02, found: 213.02

Compound **4**

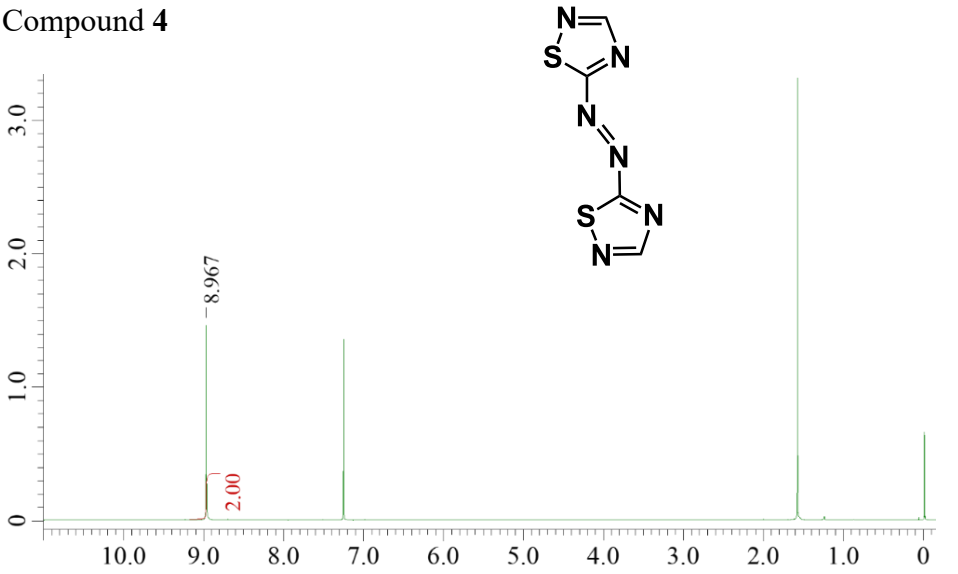

Figure 17: ^{1}H NMR of compound **4** in $CDCl_3$.

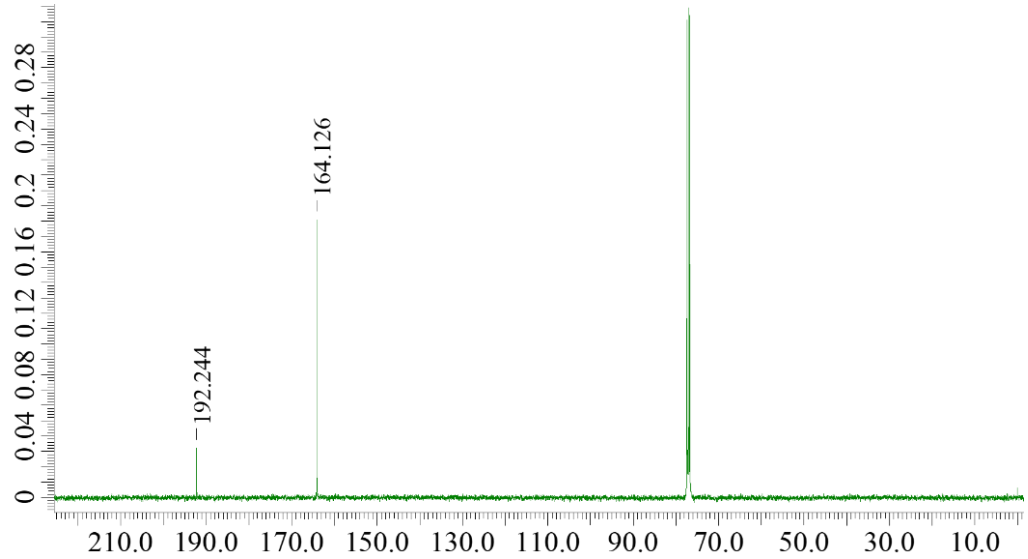

Figure 18: ^{13}C NMR of compound **4** in $CDCl_3$.

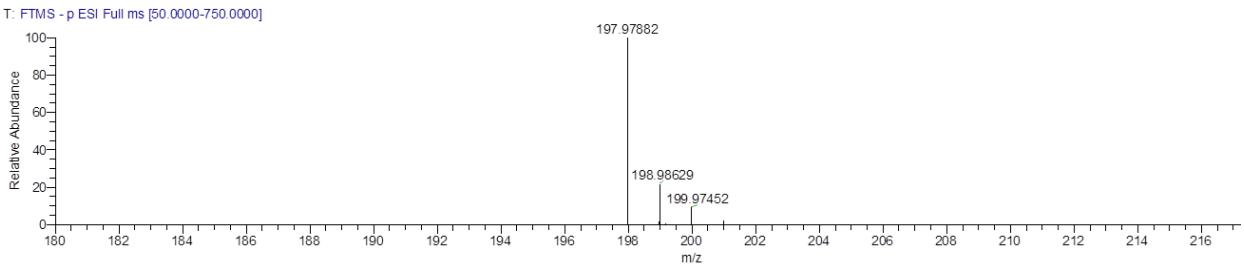

Figure 19: High-resolution mass spectra (ESI) of compound **4.** *m/z* $[M]^+$ calculated for $C_4H_2N_6S_2$: 197.98, found: 197.97

Compound **5**

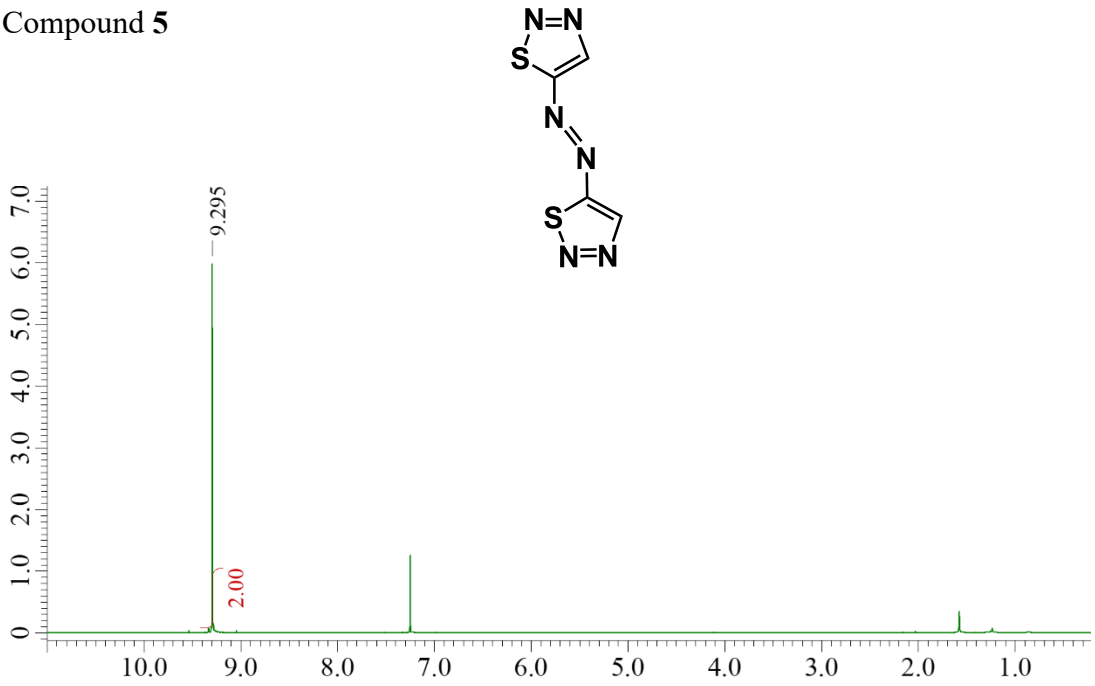

Figure 20: ^{1}H NMR of compound **5** in $CDCl_3$.

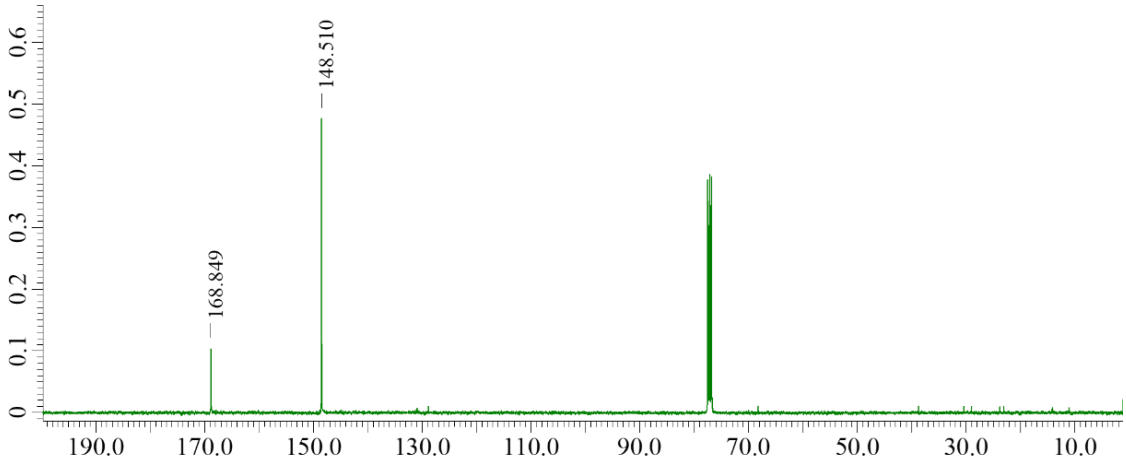

Figure 21: ^{13}C NMR of compound **5** in $CDCl_3$.

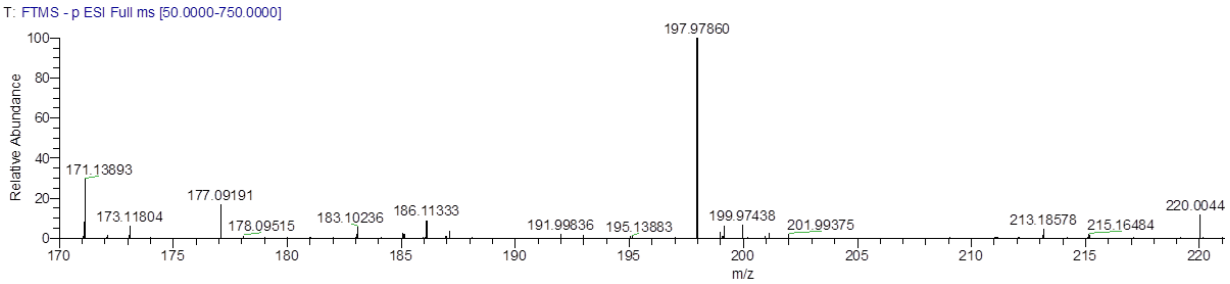

Figure 22: High-resolution mass spectra (ESI) of compound **5.** *m/z* $[M]^+$ calculated for $C_4H_2N_6S_2$: 197.98, found: 197.97

Compound **6**

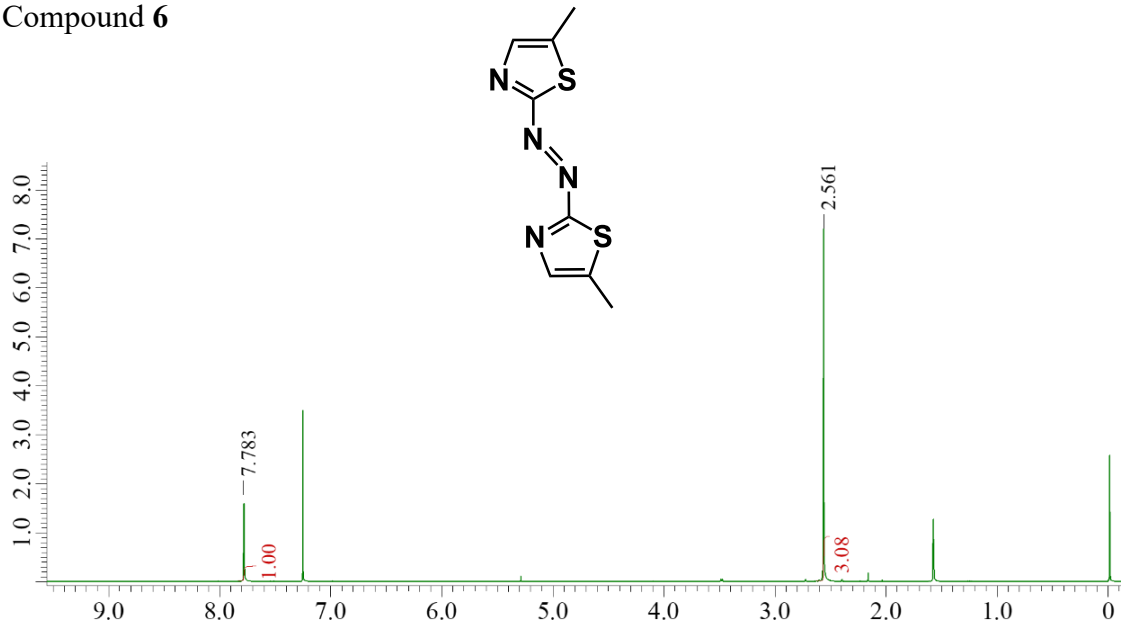

Figure 23: ^{1}H NMR of compound **6** in $CDCl_3$.

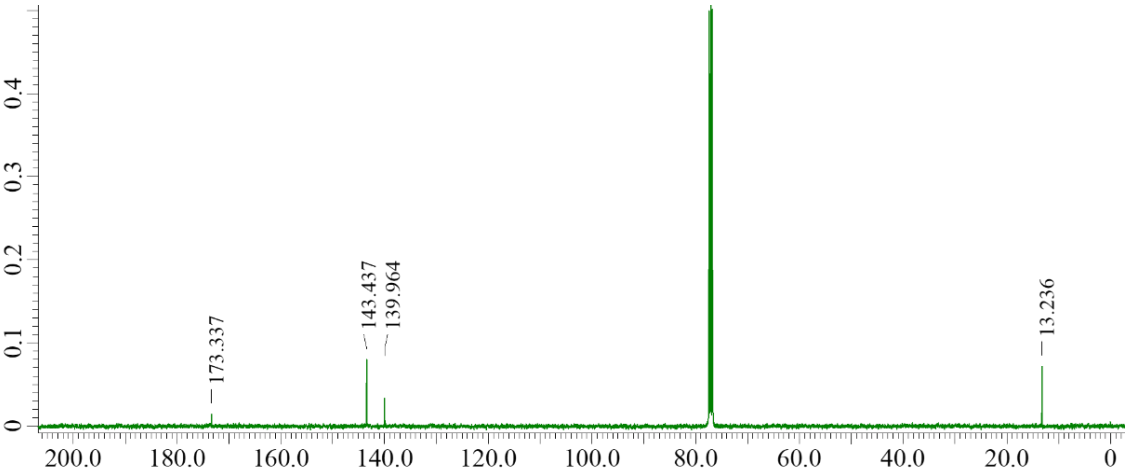

Figure 24: ^{13}C NMR of compound **6** in $CDCl_3$.

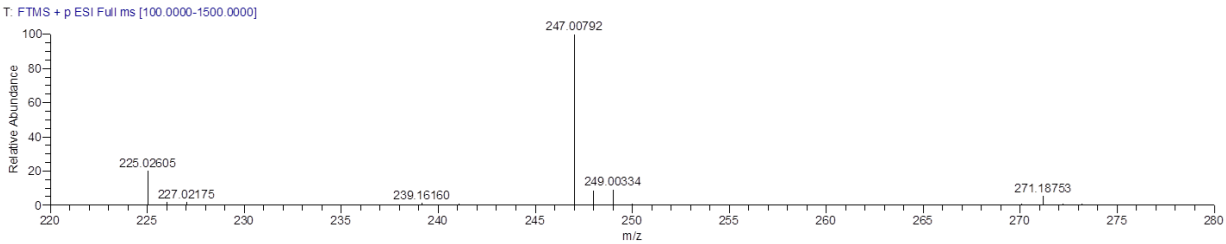

Figure 25: High-resolution mass spectra (ESI) of compound **6.** *m/z* $[M + Na]^+$ calculated for $C_8H_8N_4S_2$: 247.01, found: 247. 01

Compound **7**

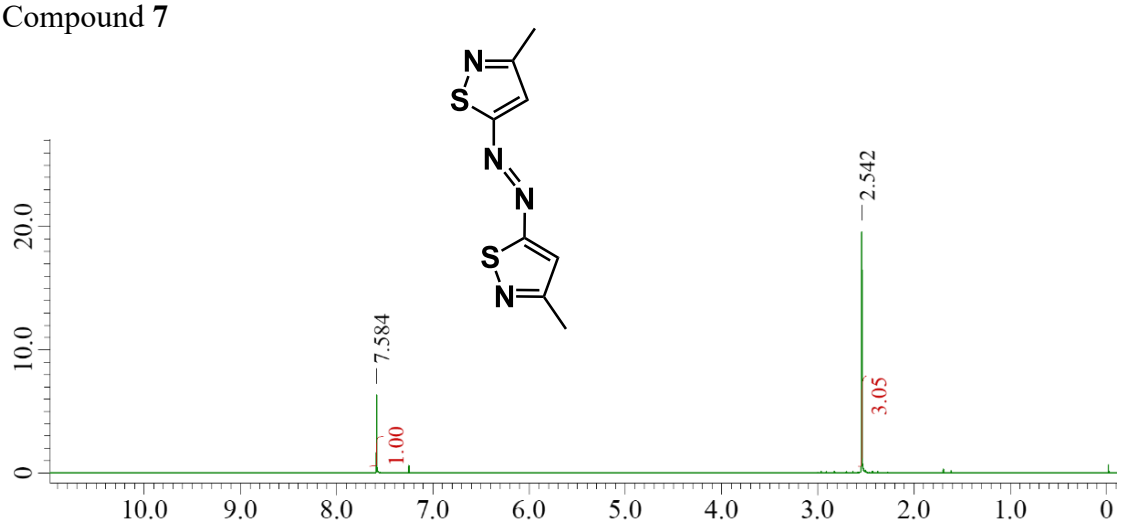

Figure 26: ^{1}H NMR of compound **7** in $CDCl_3$.

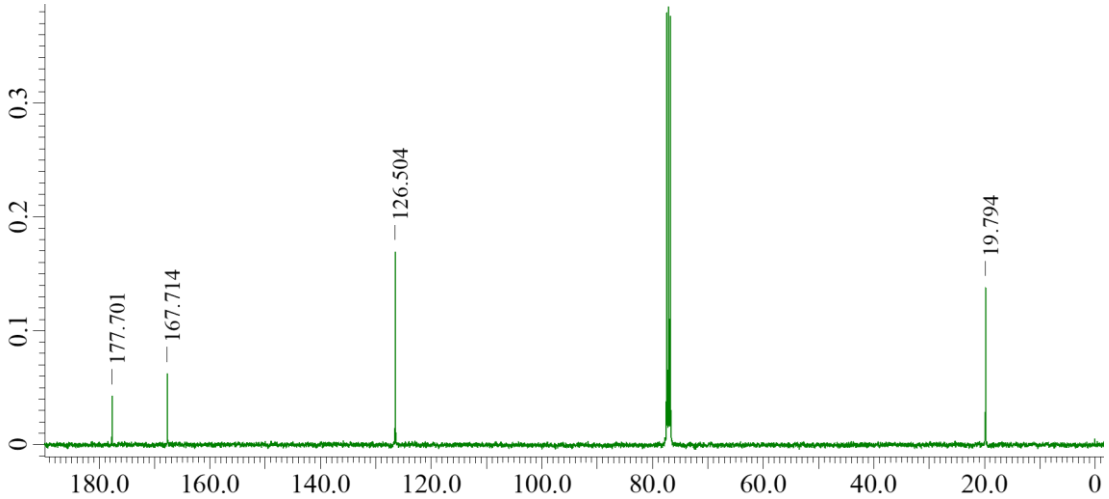

Figure 27: ^{13}C NMR of compound **7** in $CDCl_3$.

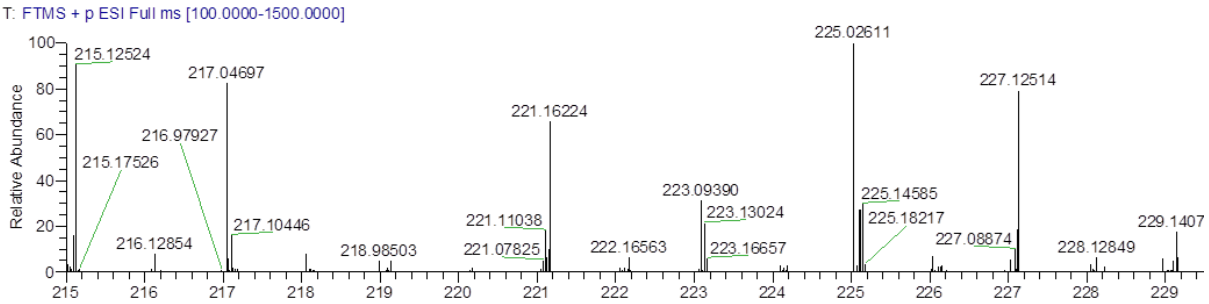

Figure 28: High-resolution mass spectra (ESI) of compound **7.** *m/z* $[M + H]^+$ calculated for $C_8H_8N_4S_2$: 225.03, found: 225.02, 227.13

Compound **8**

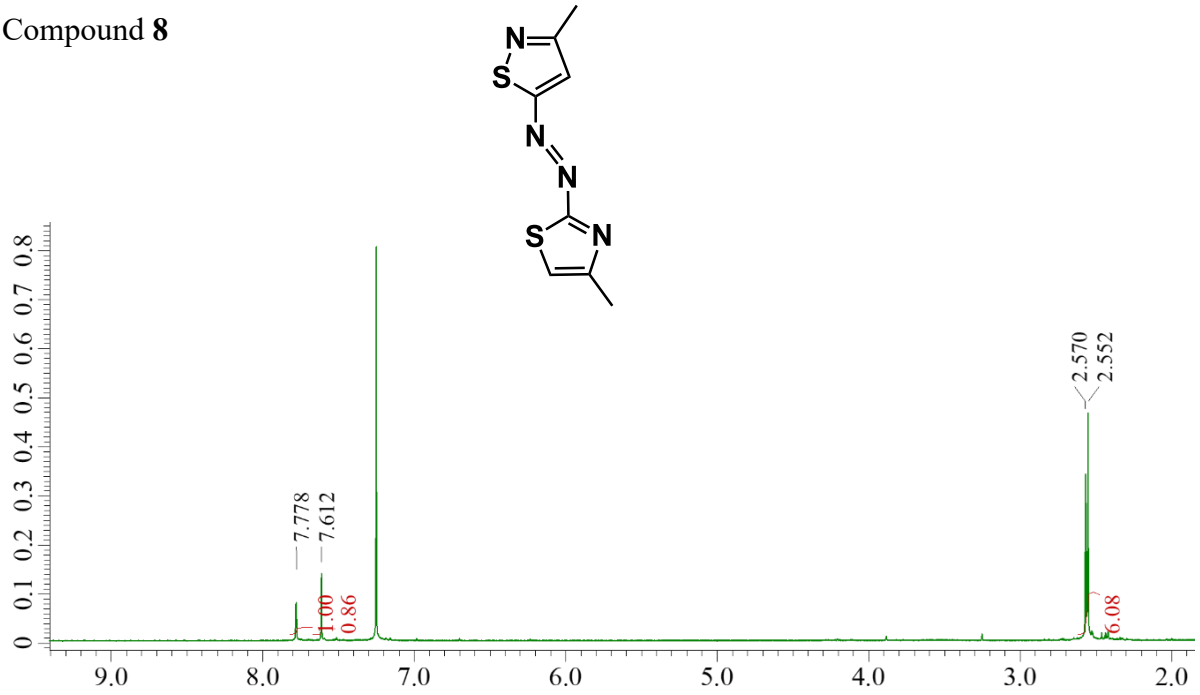

Figure 29: ^{1}H NMR of compound **8** in $CDCl_3$.

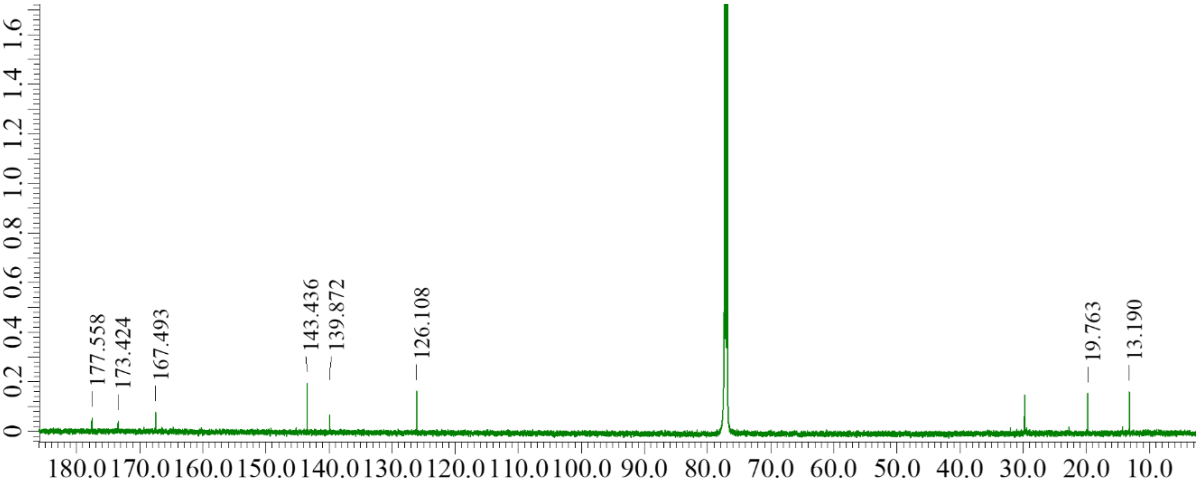

Figure 30: ^{13}C NMR of compound **8** in $CDCl_3$.

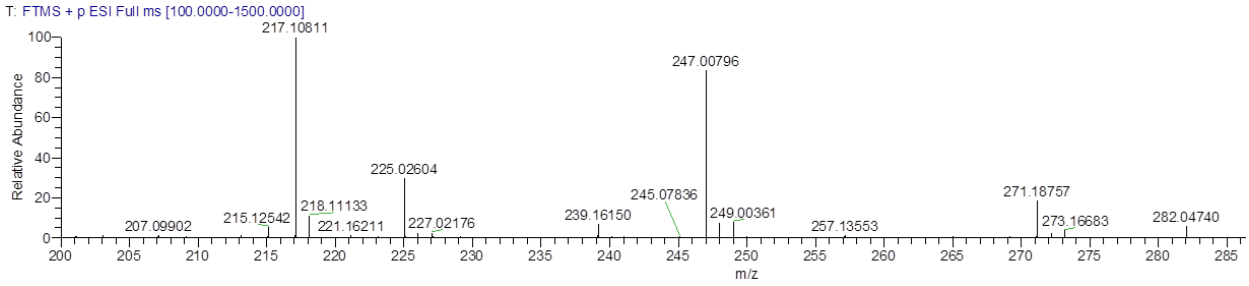

Figure 31: High-resolution mass spectra (ESI) of compound **8.** *m/z* $[M + Na]^+$ calculated for $C_8H_8N_4S_2$: 247.01, found: 247. 01

2.5 Measurement of isomer conversion at PSS

To determine the composition of *trans* and *cis* isomers at the photostationary state, I used two methods:[1]H NMR spectroscopy for compounds **1**, **2**, **3**, and **7**, and absorption spectroscopy for compounds **4**, **5**, **6**, and **8**. Due to the short half-lives of compounds **4**, **5**, **6** and **8**, [1]H NMR was not suitable, so absorption spectroscopy was used to calculate their isomer ratios.

A.) Isomer conversion measurement at PSS by [1]H NMR (compound 1,2,3 and 7).

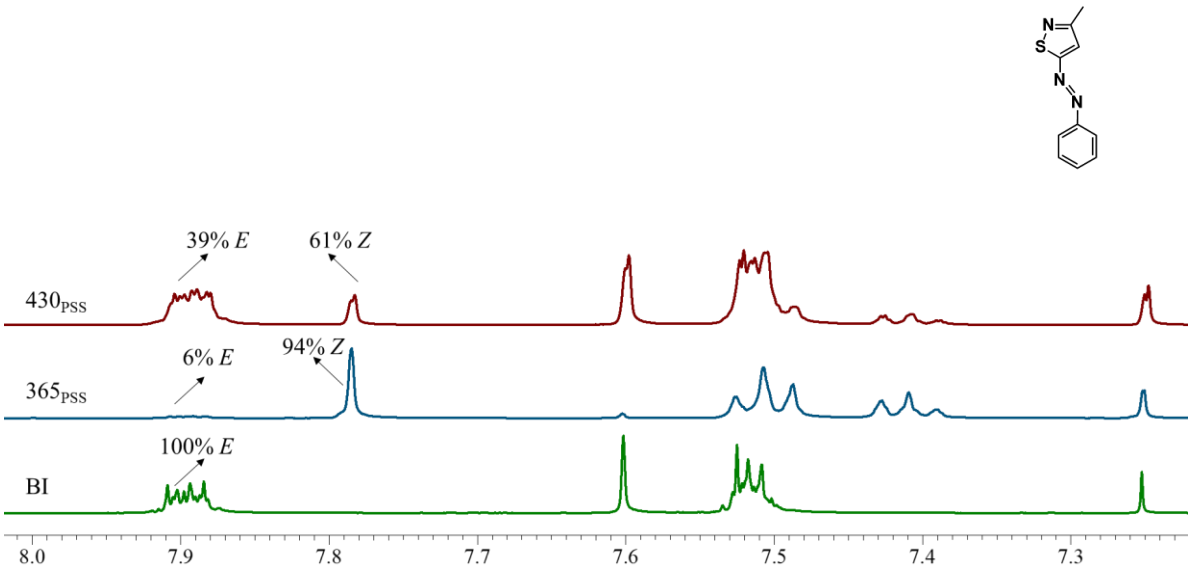

Figure 32: [1]H NMR spectra (400 MHz, $CDCl_3$) of compound **1** obtained before irradiation (BI) and irradiations at PSS of 365 nm (365_{PSS}) and 525 nm (430_{PSS}) at 25 °C.

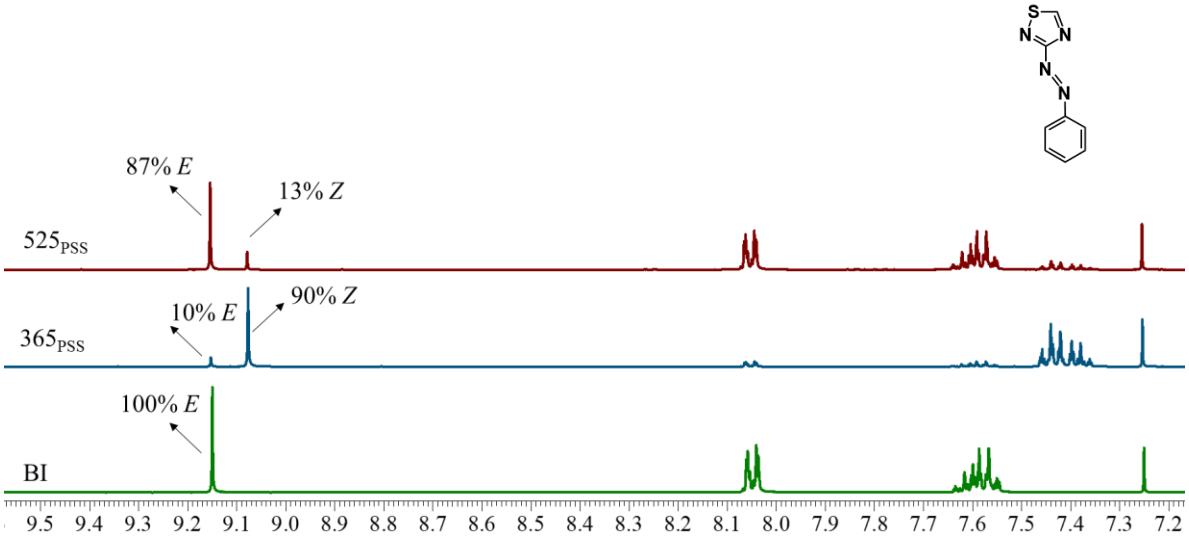

Figure 33: ^{1}H NMR spectra (400 MHz, $CDCl_3$) of compound **2** obtained before irradiation (BI) and irradiations at PSS of 365 nm (365_{PSS}) and 525 nm (525_{PSS}) at 25 °C.

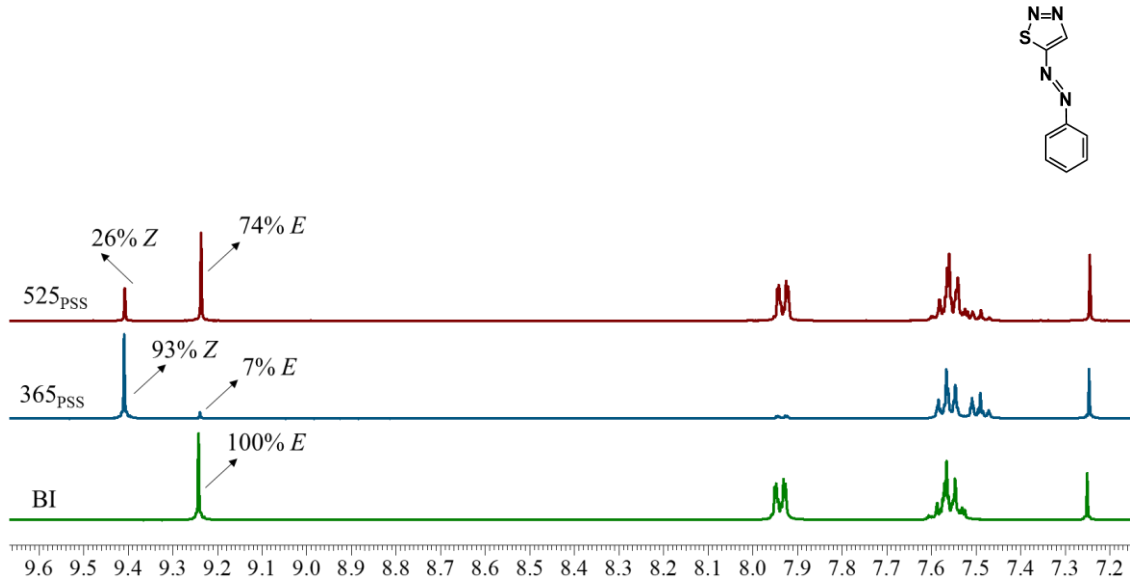

Figure 34: ^{1}H NMR spectra (400 MHz, $CDCl_3$) of compound **3** obtained before irradiation (BI) and irradiations at PSS of 365 nm (365_{PSS}) and 525 nm (525_{PSS}) at 25 °C.

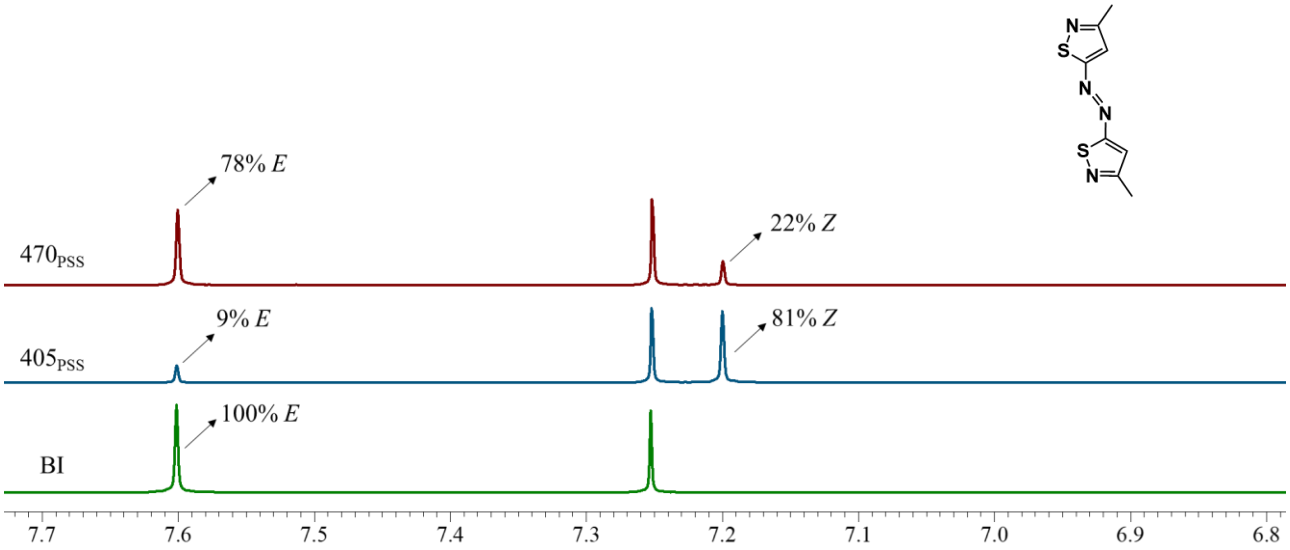

Figure 35: ^{1}H NMR spectra (400 MHz, $CDCl_3$) of compound **7** obtained before irradiation (BI) and irradiations at PSS of 405 nm (405_{PSS}) and 470 nm (470_{PSS}) at 25 °C.

B.) Isomer conversion measurement at PSS by absorption spectra (compound 4,5,6 and 8)

When the extinction coefficient of the *Z* isomer of the photoswitch (ε_Z) at λ_{max} was greater than zero, the minimum conversion (%) from *E* to *Z* at PSS were calculated as $\frac{A_0 - A_{PSS}}{A_0} \times 100$ using the following equation:

$$Conversion\ (\%) from\ E\ to\ Z \quad = \frac{A_{PSS} - A_{PSS,E}}{A_0} \times 100 = \frac{A_0 - \left(A_{PSS} - A_{PSS,Z}\right)}{A_0} \times 100$$

$$> \frac{A_0 - A_{PSS}}{A_0} \times 100$$

A_0 Absorbance at initial state (100% *trans*) at λ_{max}

A_{PSS} Absorbance at PSS at λ_{max}

$A_{PSS,\,E}$ A portion of absorbance at PSS at λ_{max}, contributed by *E* isomer

$A_{PSS,\,Z}$ A portion of absorbance at PSS at λ_{max}, contributed by *Z* isomer

2.6 Measurement of thermal half-life

A freshly prepared solution was irradiated at 365 nm, or 405 or 430 nm until its photostationary states and immediately kept for thermal back *Z–E* isomerization in dark at 25 °C. In all cases, 6–8 spectra at fixed time intervals were recorded under dark condition to minimize the effect of light beam on thermal back isomerization. Then, a first order rate constant (k) for the thermal back *Z–E* isomerization reaction was obtained using the equation:

$$ln\frac{A_t}{A_0} = ln\frac{Abs(BI) - Abs(time)}{Abs(BI) - Abs(PSS)} = -kt$$

Abs(BI) = absorbance at initial state at λ_{max}.

Abs(PSS) = absorbance at photostationary state at λ_{max}.

Abs(time) = absorbance at λ_{max} at different time interval for thermal back isomerization.

For a first order reaction, half-life ($t_{1/2}$) can be calculated using the equation:

$$t_{1/2} = 0.693/k$$

2.7 Single crystal X-ray structure analysis

I obtained single crystals of the *trans* isomers (compounds **2**–**6**) and *cis* isomers (compounds **2** and **3**) using the vapor diffusion method at low temperature.

General procedure for the crystallization of compounds 2, 3, 4, 5, 6 and 8

A small vial containing the compound dissolved in chloroform (10 mmol, 200 μL) is placed inside a larger container with hexane (70 mL). The system is maintained at -20 °C for 2 days, ensuring it is well-sealed to prevent solvent evaporation. During this time, the vapor concentration of hexane increases, causing the solubility of the compound in chloroform to gradually decrease, leading to the slow precipitation of crystals from the solution.

Crystallization of *cis* isomer of compounds 2 and 3

Photoswitch solution in small vial was irradiated with 365 nm light until reaching photostationary state and immediately transferred into the larger vial containing hexane and left to crystallize as described in the general procedure.

This technique allowed for the slow and controlled crystallization of the compounds, enabling the isolation of high-quality single crystals suitable for structural analysis. Cryoloop was used to mount the single crystals. Crystallographic data was collected using a Rigaku XtaLab Synergy diffractometer with a single microfocus Mo Kα X-ray radiation source (PhotonJet-S), equipped with a Hybrid Pixel (HyPix) Array detector (HyPix-6000HE). Data collection, cell refinement,

and data reduction were carried out with CrysalisPRO (Rigaku Oxford Diffraction, 2017). The initial structure was solved by SHELXT and expanded using Fourier techniques and refined on F^2 by the full-matrix least-squares method SHELXL2018/3 package compiled into OLEX2 package. All parameters were refined using anisotropic temperature factors, except for hydrogen atoms, which were refined using the riding model, with a fixed C–H bond distance.

CCDC 2371070 for **2** (*trans*), 2371071 for **2** (*cis*), 2371069 for **3** (*trans*), 2371067 for **3** (*cis*), 2371065 for **4,** 2371066 for **5,** 2371068 for **6,** 2371072 for **8** contain the supplementary crystallographic data for this study.

2.8 DFT calculation

Density Functional Theory (DFT) was employed to predict the electronic and geometric properties of the photoswitches. Theoretical calculations were performed using Gaussian 09 (Revision D.01). GaussView 6.0 was used to draw and visualize the molecular structures and to feed the inputs. Density functional theory (DFT) and time dependent density functional theory (TDDFT) were employed to optimize the geometries and to obtain the electronic transition in the ground state, respectively. The 6-31+G(d,p) basis set with Becke's three-parameter hybrid exchange and the Lee-Yang-Parr's correlation functional (B3LYP) was used for geometry optimization. The solvent stabilization of different isomers was incorporated by considering integral equation formalism-polarizable continuum model (IEF-PCM) and choosing acetonitrile as medium.

3. Results and discussions

3.1 Screening λ_{max} of the photoswitches by DFT calculations

To study the light absorption properties (λ_{max}) of various photoswitchable molecules, I designed 24 compounds containing sulfur (S), nitrogen (N), or oxygen (O) heteroatoms within the five-membered aromatic ring. We conducted DFT calculations to gain insight into their absorption maxima, providing predictions on how structural variations affect light absorption (Table 1). By predicting the λ_{max} values, DFT provided a theoretical understanding of how these compounds respond to light irradiation, which is vital for designing photoswitches that operate under specific light conditions The molecules were categorized into two groups based on the nature of the heteroarene and aromatic systems. The first group, photoswitches **a**–**i**, comprised molecules with a 5-membered heteroarene (R1) on one side of the azo bond (–N=N–) and a phenyl ring (R2) on the other side. This combination allows for different electronic environments across the molecule, with the heteroarene contributing to the unique light absorption properties. In contrast, the second group, photoswitches **j**–**x**, consisted of azoheteroarenes containing either identical or different 5-membered heteroarenes as both R1 and R2. This variation allowed for the exploration of how the symmetry or asymmetry of the heteroaryl groups influences the photophysical behavior, particularly the absorption maxima.

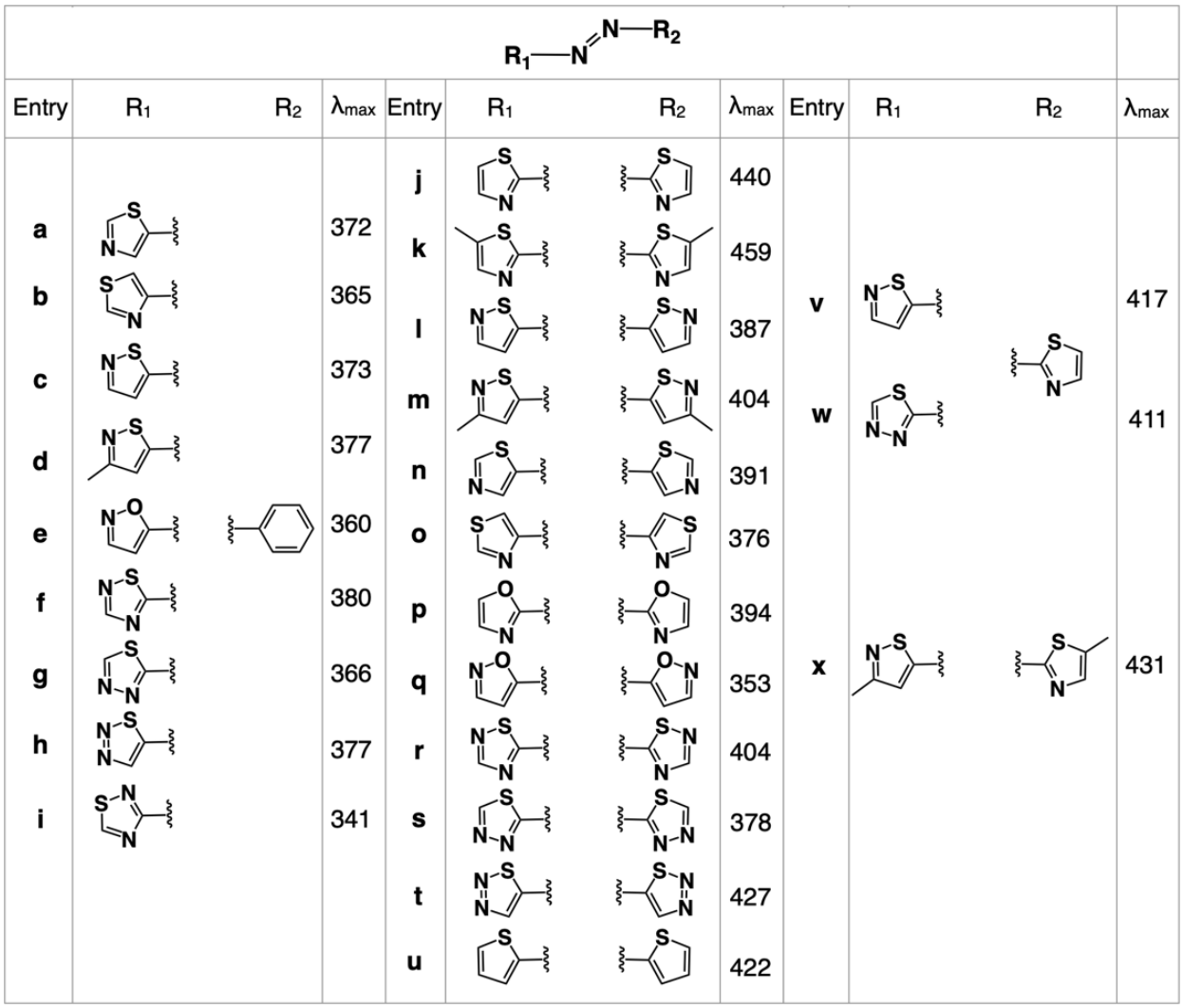

Table 1: Table showing the part of molecular structures of heteroaryl azophotoswitches designed along with their calculated λ_{max} values. R1 and R2 are phenyl or 5-membered heteroaryl units.

3.2 Synthesis

Guided by the calculated λ_{max} values, I selected eight compounds for synthesis, focusing on photoswitches with the longest and third-longest absorption maxima, represented by Entries **k** and **x**. Although azobisthiazole (Entry **j**) was calculated to have the second-highest λ_{max} at 440 nm, attempts to synthesize it by oxidizing 2-amino thiazole were unsuccessful. This was likely due to undesired oxidation occurring at the sulfur atom within the thiazole ring, which hindered the formation of the desired azo linkage.

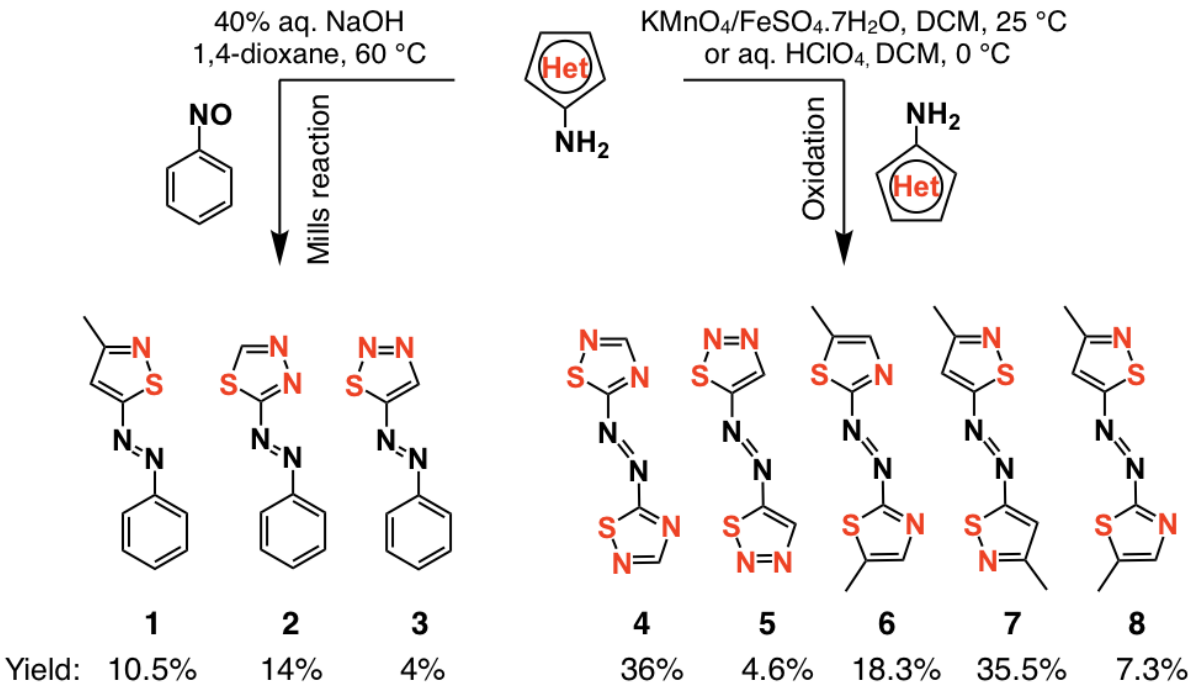

Figure 36: Synthesis of photoswitches from amino-heteroaryl derivatives via the Mills reaction with nitrosobenzene (**1**–**3**) or oxidation (**4**–**8**).

I used a one-step synthetic procedure to prepare compounds **1**–**8**, as shown in Figure 36. This method enabled direct conversion of aminoheteroaryl starting materials into the target azo compounds, reducing reaction time and eliminating intermediate purification steps. Additionally, this single-step protocol allowed flexibility to incorporate different heteroaryl groups, facilitating the synthesis of variety of azo-linked photoswitches. Compounds **1**–**3** were synthesized via Mill`s reaction using the corresponding 2-amino heteroarene derivatives and nitrosobenzene. Mill`s reaction a well-established method for forming azobenzenes by reacting aniline with nitrosobenzene. Only a few reports have been published on the synthesis of heteroaryl photoswitches via Mill's reaction. While I started with the conventional method, I optimized the reaction conditions—such as temperature, solvent, and reaction time—to successfully form the corresponding heteroaryl photoswitches. The optimization conditions are detailed in the table below (Table 2) where the first entry corresponds to a reported Mill's reaction for the synthesis of aryl pyrazole.

	Solvent	Temperature	Base	Time	Yield
1	Pyridine	80	40% aq. NaOH	12-24 hours	–
2	Pyridine	r.t	40% aq. NaOH	12-24 hours	–
3	Benzene	r.t	40% aq. NaOH	12-24 hours	–
4	Benzene	70	40% aq. NaOH	2 hours	1.40%
5	1,4-dioxane	60	40% aq. NaOH	2 hours	5.9% - 17.2%
6	1,4-dioxane	60	50% aq. NaOH	2 hours	2.20%
7	1,4-dioxane	60	40% aq. NaOH	12-24 hours	–

Table 2: Optimization of synthetic conditions for the formation of compounds **1**–**3**.

General procedure for synthesis of compounds **1-3**.

To a warm (40 °C) NaOH solution (40% aq., 1 mL), 2-amino heteroaryl compounds (2.3 mmol) in 1,4-dioxane (2.5 mL) was added and gently heated to 60 °C. Then, nitroso-benzene (2.53 mmol) was added slowly, and the mixture was stirred for 2 hours. The reaction mixture was then cooled and quenched with water and extracted with ethyl acetate (3 x 25 mL). The organic layer was washed with brine, dried over $MgSO_4$, and concentrated under reduced pressure. The target compound was then isolated by column chromatography.

This method can be applied to various heteroaryl groups, including thiazole, isothiazole, thiadiazole, isothiadiazole, isoxazole, while maintaining optimal yields.

Compounds **4**–**8** were synthesized by oxidizing the corresponding 2-amino heteroarene derivatives. A common method for synthesizing azo compounds, such as azobenzene derivatives, involves the oxidation of aromatic amines like anilines, converting the amine precursors into azo linkages (–N=N–). The direct oxidation of aromatic amines to form azo compounds can be facilitated by various oxidizing agents. To optimize the reaction conditions for heteroaryl azo synthesis, I tested a range of oxidizing agents, including sodium hypochlorite, manganese dioxide, and potassium permanganate. Through this optimization process, potassium permanganate was identified as the most effective oxidizing agent for the majority of the heteroaryl compounds synthesized. These agents were carefully evaluated for their efficiency in promoting oxidation and generating the desired azo compounds, as detailed in Table 3.

	Oxidizing agent	Equivalency	Solvent	Time	Yield
1	Sodium hypochlorite crystal	10	EtOAc	overnight	
2	Sodium hypochlorite crystal	3	DCM	1 hour	
3	Sodium hypochlorite crystal	6	EtOAc	1 hour	
4	Sodium hypochlorite crystal	5	EtOAc	1 hour	
5	Sodium hypochlorite crystal	2	dehydr.methanol	Ar cond.1 hour	
6	Sodium hypochlorite crystal	2	methanol	1 hour	
7	Sodium hypochlorite solution		EtOAc	1 hour	
8	Sodium hypochlorite solution		DCM	dark, 1 hour	
9	Sodium hypochlorite solution		water	1 hour	
10	Sodium hypochlorite solution		DCM	1 hour	36%
11	SDCl, Acetic acid		acetonitrile	1 hour	
12	Mangansese dioxide		toluene	overnight, reflux	
13	Potassium permanganate,ferrous sulfate		DCM	overnight, r.t	2.3% - 18%
14	Potassium permanganate,ferrous sulfate		DCM	overnight, reflux	0.018

Table 3: Optimization of synthetic conditions for the formation of compounds **4**–**8**.

General procedures for synthesis of compounds **4**-**8**.

(1) To cold sodium hypochlorite solution, cool suspension of aminothiadiazole (4.9 mmol) in dichloromethane (15 mL) was added little by little followed by stirring for 1 hour at 0 ˚C. The reaction mixture was quenched with water and extracted with dichloromethane (3 x 25 mL). The organic layer was washed with brine, dried over $MgSO_4$, and concentrated *in vacuo*. The target compound was then isolated by column chromatography.

(2) A heteroaryl amino compound (5 mmol) was dissolved in dichloromethane. Potassium permanganate (15 mmol) and ferrous sulfate heptahydrate (10 mmol) were ground together until

homogenous. The resulting powder was added to the dichloromethane solution. The mixture was stirred for 24 hours at room temperature. Afterward, the reaction mixture was filtered through celite, and the solvent evaporated. Finally, the target compound was isolated using column chromatography.

A methyl substituent at position 5 of the amino thiazole gave azobis(methylthiazole) (compound **6**) in 18% yield. This compound can also be synthesized by a multiple-step reaction as appeared in a recent thesis report.[28] The NMR, Mass and X-ray analysis confirmed the structures of target compounds **1**–**8** (Experimental section). By prioritizing these compounds, I intended to explore their effectiveness as photoswitchable systems with improved light absorption.

3.3 Photophysical studies

The performance of photoswitches **1**–**8** was evaluated using key parameters such as maximum wavelength of absorption, composition of isomers at photostationary state and thermal stability of the *cis* isomers. The absorption spectra revealed strong absorption bands (λ_{max} = 332–429 nm) assignable to π-π* electron transition bands. Notably, some of the photoswitches exhibited λ_{max} values within the visible light range, which is particularly relevant for applications where visible light activation is advantageous. To study their photoisomerization behavior, I recorded the absorption spectra of the photoswitches under light irradiation. Upon irradiation with light of suitable wavelengths (365, 405, 430, 450, or 470 nm), significant changes were observed in the absorption bands, indicating isomerization from the *trans* isomer to the *cis* isomer. Reverse isomerization occurred either thermally or upon irradiation with longer-wavelength light (430, 470, 525, or 568 nm). To quantify the composition of *trans* and *cis* isomers at the photostationary state under different wavelengths, I employed two approaches: ^{1}H NMR spectroscopy for compounds **1**, **2**, **3** and **7**, and absorption spectroscopy for compounds **4**, **5**, **6** and **8**. Additionally, I studied the thermal stability of the *cis* isomers by monitoring the changes in absorbance at their respective λ_{max} after reaching a *cis*-rich PSS. Assuming compounds followed first-order thermal isomerization kinetics half-lives of the *cis* isomers were calculated.

Compound **1**: This compound, featuring an isothiazole group linked to a phenyl ring via an azo bond. It exhibits a λ_{max} of 332 nm in the π-π* transition band and 448 nm in the n-π* transition band for the stable *trans* isomer, with a calculated λ_{max} of 377 nm (π-π* transition). For the *cis* isomer, the λ_{max} in the n-π* transition band is at 448 nm. Under 365 nm UV light, it efficiently photoisomerizes to its *cis* form, achieving 94% *cis* isomer at PSS. Reverse isomerization occurs under 430 nm light or thermally yielding 61% *trans* isomer at PSS. Among the studied compounds, it stands out with the longest half-life ($t_{1/2}$ = 45.2 hours) for their *cis*-isomers.

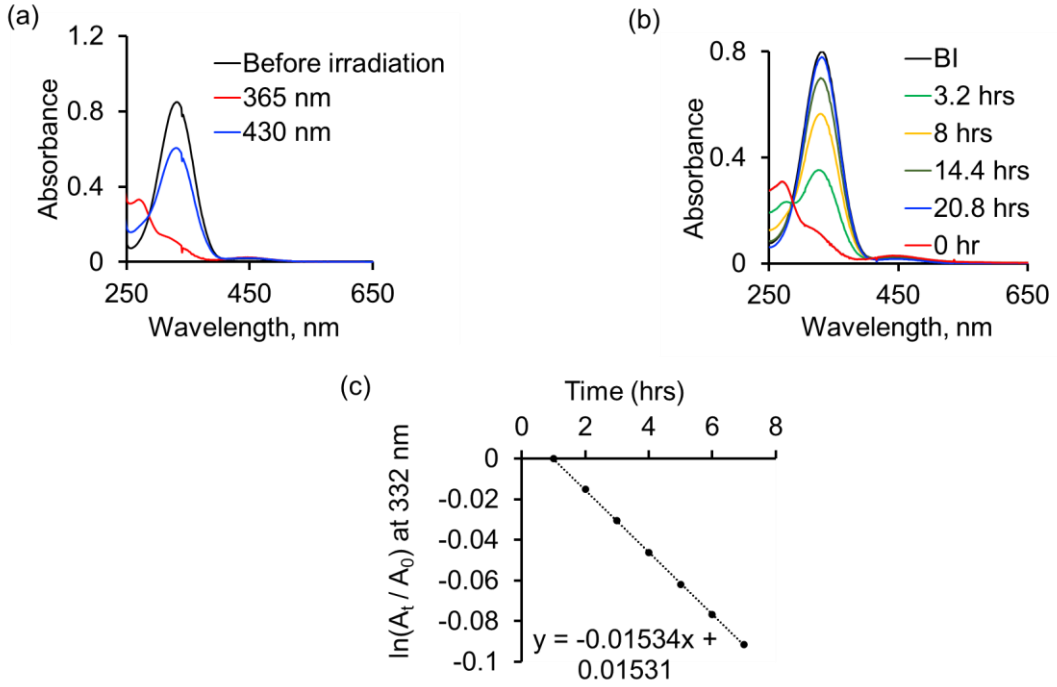

Figure 37: (a) UV−visible absorption spectra of **1** in acetonitrile at 25 °C before irradiation (BI, black line) and at the *cis*-rich PSS under 365 (365_{PSS}; red line) and at *trans*-rich PSS under 430 nm irradiation (430_{PSS}; blue line). (b) Thermal back-isomerization of compound **1** in acetonitrile at 50 °C: spectra before irradiation (BI), at *cis*-rich PSS (365_{PSS}, 0 hr), and at the *trans*-rich state after thermal relaxation (20.8 hours) (c) Linear fit of absorbance change at 332 nm over time for compound **1** at 25 °C showing the rate constant *k* (= slope) and $t½$ = 45.2 hours.

Compound **2**: This compound, featuring 1,3,4-thiadiazole ring linked to a phenyl ring via an azo bond. It exhibits a λ_{max} of 334 nm in the π-π* transition band and 448 nm in the n-π* transition band for the stable *trans* isomer, with a calculated λ_{max} of 366 nm (π-π* transition). For the *cis* isomer, the λ_{max} in the n-π* transition band is at 448 nm. Under 365 nm UV light, it efficiently photoisomerizes to its *cis* form, achieving 90% cis isomer at PSS. Reverse isomerization occurs under 430 nm light or thermally yielding 87% *trans* isomer at PSS. Compound **2** shows a half-life of 29.4 hours for their *cis*-isomers.

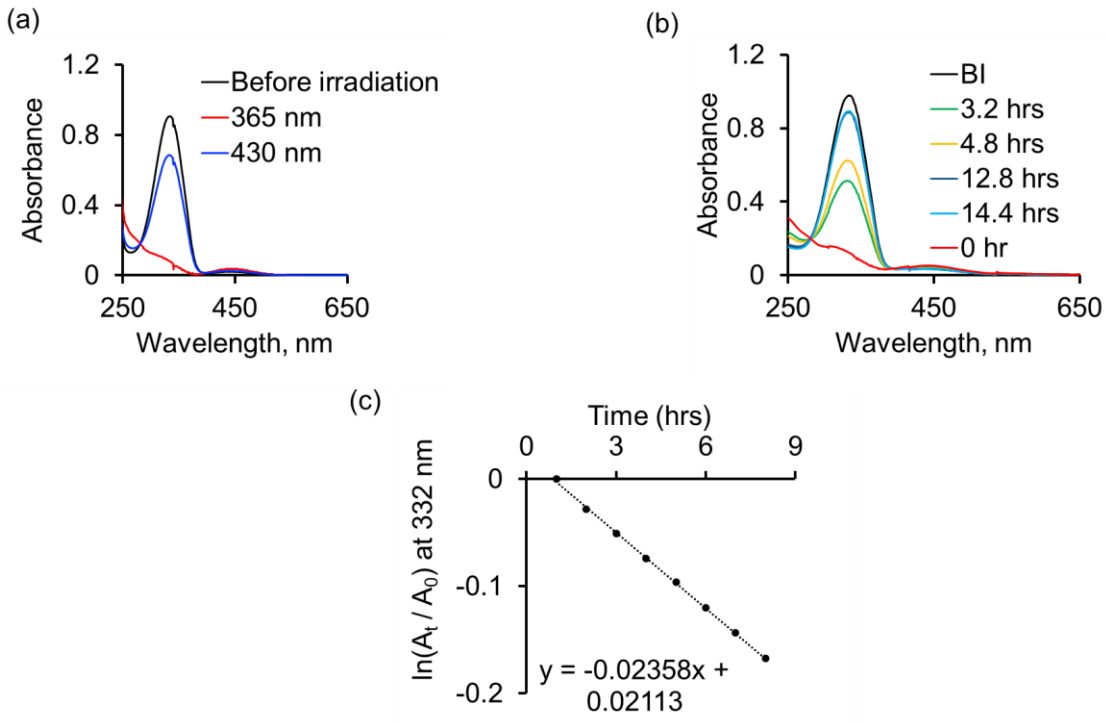

Figure 38: (a) UV−visible absorption spectra of **2** in acetonitrile at 25 °C before irradiation (BI, black line) and at the *cis*-rich PSS under 365 (365_{PSS}; red line) and at *trans*-rich PSS under 430 nm irradiation (430_{PSS}; blue line). (b) Thermal back-isomerization of compound **2** in acetonitrile at 50 °C: spectra before irradiation (BI), at *cis*-rich PSS (365_{PSS}, 0 hr), and at the *trans*-rich state after thermal relaxation (14.4 hours) (c) Linear fit of absorbance change at 332 nm over time for compound **2** at 25 °C showing the rate constant *k* (= slope) and $t_{½}$ = 29.4 hours.

Compound **3**: This compound, featuring 1,2,3-thiadiazole ring linked to a phenyl ring via an azo bond. It exhibits a λ_{max} of 345 nm in the π-π* transition band and 453 nm in the n-π* transition band for the stable *trans* isomer, with a calculated λ_{max} of 377 nm (π-π* transition). For the *cis* isomer, the λ_{max} in the n-π* transition band is at 458 nm. Under 365 nm UV light, the compound undergoes efficient photoisomerization to its *cis* form, reaching 93% *cis* isomer at the photostationary state. Reverse isomerization is by 430 nm light or occurs thermally, producing 74% *trans* isomer at PSS. Compound **3** shows a half-life of 24.3 hours for their *cis*-isomers.

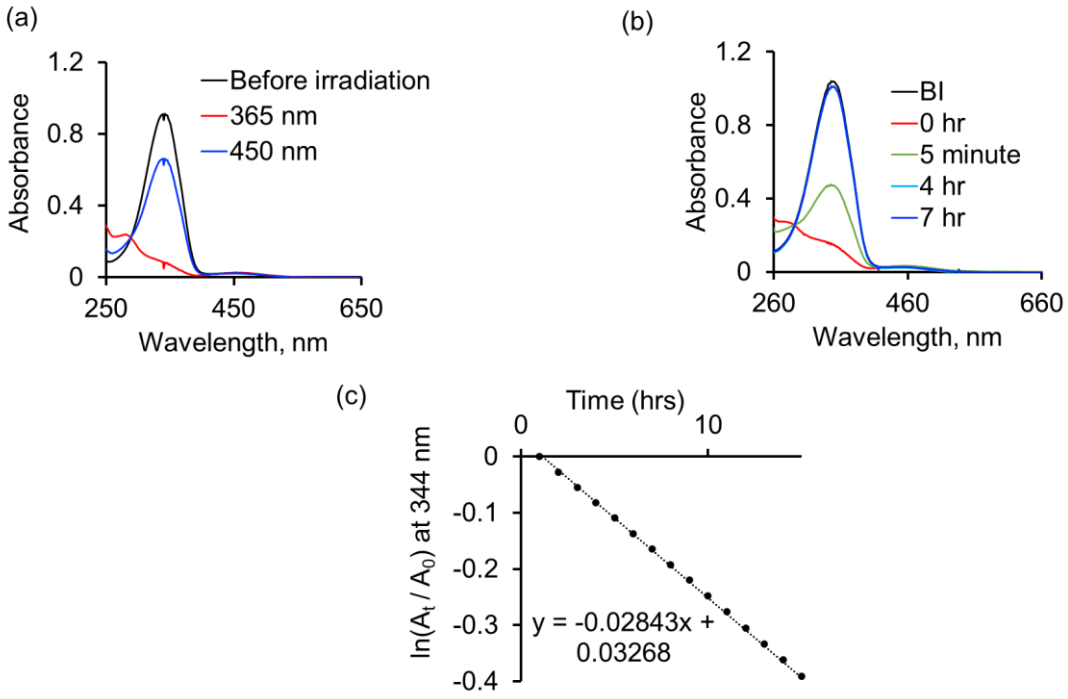

Figure 39: (a) UV−visible absorption spectra of **3** in acetonitrile at 25 °C before irradiation (BI, black line) and at the *cis*-rich PSS under 365 (365_{PSS}; red line) and at *trans*-rich PSS under 450 nm irradiation (450_{PSS}; blue line). (b) Thermal back-isomerization of compound **3** in DMSO at 25 °C: spectra before irradiation (BI), at *cis*-rich PSS (365_{PSS}, 0 hr), and at the *trans*-rich state after thermal relaxation (7 hours) (c) Linear fit of absorbance change at 344 nm over time for compound **3** at 25 °C showing the rate constant *k* (= slope) and $t½$ = 24.3 hours.

Compound **4**: This symmetric compound features two 1,2,4-thiadiazole rings connected via an azo bond. It exhibits a λ_{max} of 362 nm in the π-π* transition band and 483 nm in the n-π* transition band for the stable *trans* isomer, with a calculated λ_{max} of 404 nm (π-π* transition). For the *cis* isomer, the λ_{max} in the n-π* transition band is at 484 nm. Under 405 nm visible light irradiation, it efficiently photoisomerizes to its *cis* form, achieving >58% *cis* isomer at PSS. Reverse isomerization occurs under 525 nm light yielding >95% *trans* isomer at PSS. Compounds **4** exhibits remarkably short half-lives for its *cis* isomers, too brief to be accurately quantified using a conventional spectrophotometer. These half-lives were estimated to be only a few seconds, indicating rapid thermal relaxation of the *cis* form back to the *trans* configuration.

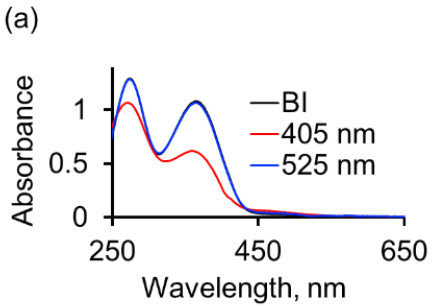

Figure 40: (a) UV−visible absorption spectra of **4** in acetonitrile at 25 °C before irradiation (BI, black line) and at the *cis*-rich PSS under 405 (405_{PSS}; red line) and at *trans*-rich PSS under 525 nm irradiation (525_{PSS}; blue lines).

Compound **5**: This is a symmetric compound, featuring two 1,2,3-thiadiazole ring linked via an azo bond. It exhibits a λ_{max} of 343 nm in the π-π* transition band and 450 nm in the n-π* transition band for the stable *trans* isomer, with a calculated λ_{max} of 427 nm (π-π* transition). For the *cis* isomer, the λ_{max} in the n-π* transition band is at 450 nm. Under 365 nm UV light irradiation, it efficiently photoisomerizes to its *cis* form, achieving >70% *cis* isomer at PSS. Reverse isomerization occurs under 470 nm light yielding >77% *trans* isomer at PSS. Compounds **5** exhibited a half-life of 3 minutes for their *cis*-isomers.

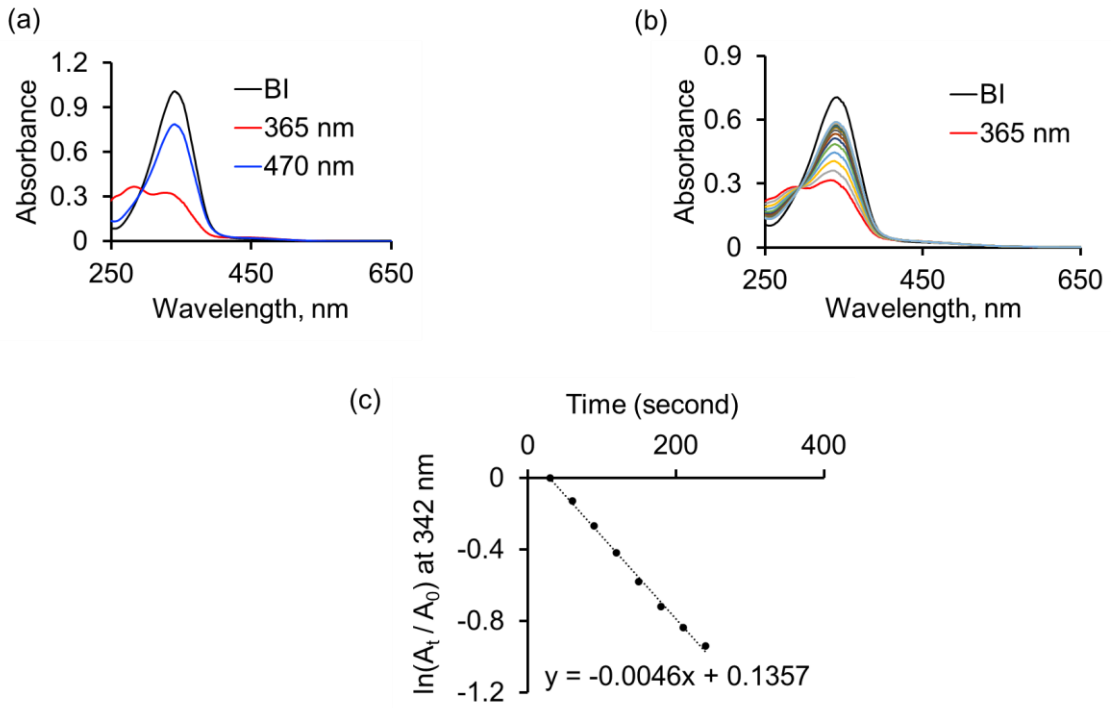

Figure 41: (a) UV−visible absorption spectra of **5** in acetonitrile at 25 °C before irradiation (BI, black line) and at the *cis*-rich PSS under 365 (365_{PSS}; red line) and at *trans*-rich PSS under 470 nm irradiation (470_{PSS}; blue line). (b) Thermal back-isomerization of compound **5** in acetonitrile at 25 °C: spectra before irradiation (BI), at *cis*-rich PSS (365_{PSS}, 0 hr), and at the *trans*-rich state after thermal relaxation (c) Linear fit of absorbance change at 342 nm over time for compound **5** at 25 °C showing the rate constant *k* (= slope) and $t½$ = 3 minutes.

Compound **6**: This is a symmetric compound, featuring two methyl thiazole rings linked via an azo bond. It exhibits a λ_{max} of 429 nm in the π-π* transition band for stable *trans* isomer, with a calculated λ_{max} of 459 nm (π-π* transition). For the *cis* isomer, the λ_{max} in the n-π* transition band is at 535 nm. Under 430 nm visible light irradiation, it efficiently photoisomerizes to its *cis* form, achieving >70% *cis* isomer at PSS. Reverse isomerization occurs under 568 nm light yielding >93% *trans* isomer at PSS. Compounds **6** exhibited relatively short half-lives of their *cis*-isomers, so brief that their changes could not be accurately tracked by a conventional spectrophotometer. It was estimated that they have half-lives of approximately several seconds.

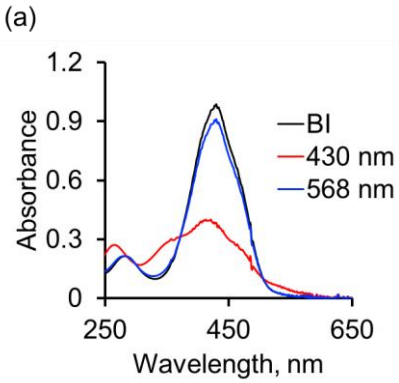

Figure 42: (a) UV−visible absorption spectra of **6** in acetonitrile at 25 °C before irradiation (BI, black line) and at the *cis*-rich PSS under 430 (430_{PSS}; red line) and at *trans*-rich PSS under 568 nm irradiation (568_{PSS}; blue lines).

Compound **7**: This is a symmetric compound, featuring two methyl isothiazole rings linked via an azo bond. It exhibits a λ_{max} of 338 nm in the π-π* transition band and 463 nm in the n-π* transition band for the stable *trans* isomer, with a calculated λ_{max} of 404 nm (π-π* transition). For the *cis* isomer, the λ_{max} in the n-π* transition band is at 460 nm. Under 405 nm visible light irradiation, it efficiently photoisomerizes to its *cis* form, achieving 81% *cis* isomer at PSS. Reverse isomerization occurs under 470 nm light yielding 74% *trans* isomer at PSS. Compounds **7** exhibited a half-life of 2.9 minutes of their *cis*-isomers.

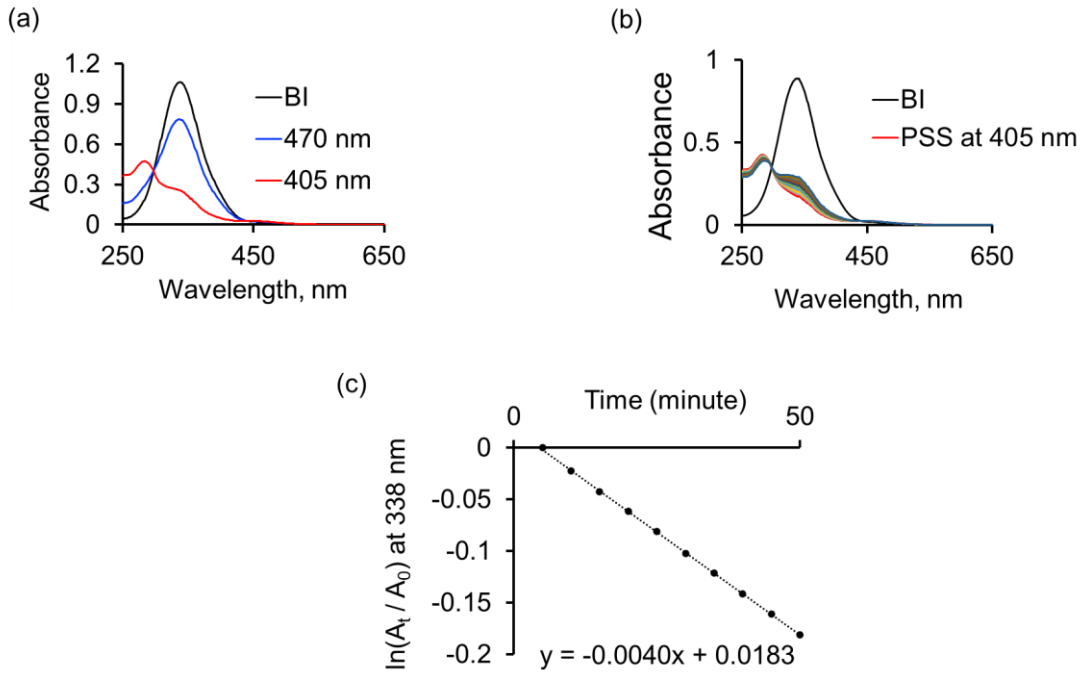

Figure 43: (a) UV−visible absorption spectra of **7** in acetonitrile at 25 °C before irradiation (BI, black line) and at the *cis*-rich PSS under 405 (405_{PSS}; red line) and at *trans*-rich PSS under 470 nm irradiation (470_{PSS}; blue line). (b) Thermal back-isomerization of compound **7** in acetonitrile at 25 °C: spectra before irradiation (BI), at *cis*-rich PSS (405_{PSS}, 0 hr), and at the *trans*-rich state after thermal relaxation (c) Linear fit of absorbance change at 338 nm over time for compound **7** at 25 °C showing the rate constant k (= slope) and $t½ = 2.9$ minutes.

Compound **8**: This is an asymmetric compound, featuring methyl thiazole rings linked to methyl isothiazole via an azo bond. It exhibits a λ_{max} of 399 nm in the π-π* transition band stable *trans* isomer, with a calculated λ_{max} of 431 nm (π-π* transition). Compound **8** isomerized efficiently from *trans* to *cis* under various visible light irradiation achieving >73% *cis* isomer at PSS with 430 nm light, >66% *cis* at PSS with 450 nm, and >47% *cis* at PSS with 470 nm. Under 525 nm light, compound **8** gave >83% *trans* isomer at PSS. Compounds **8** exhibited a half-life of 2.7 minutes of their *cis*-isomers.

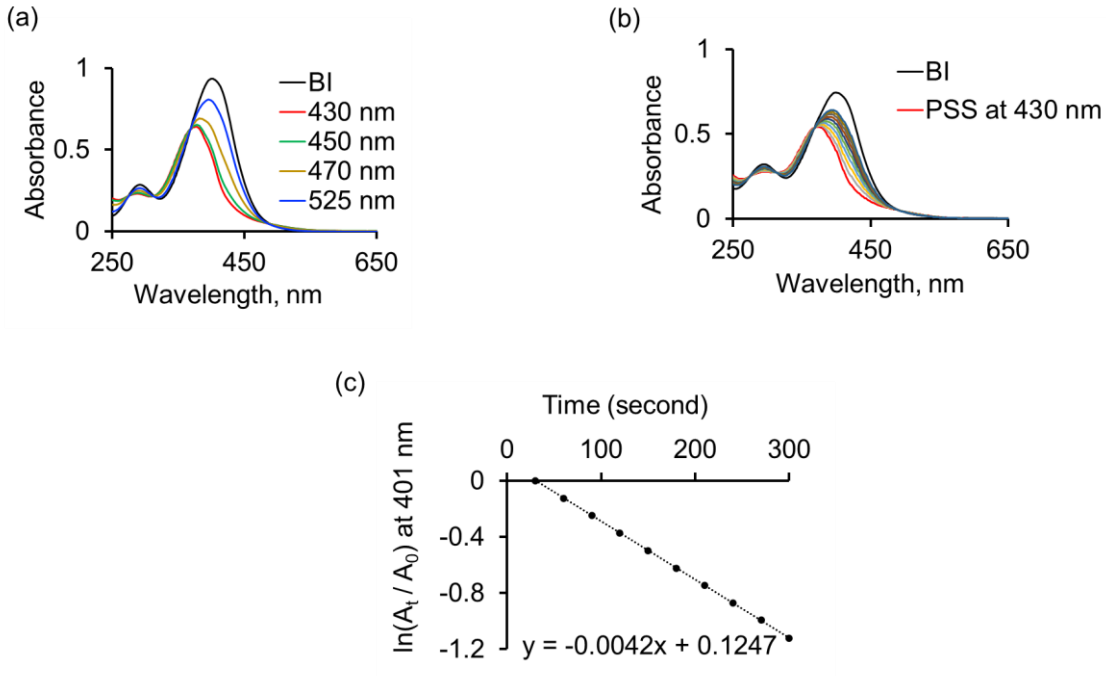

Figure 44: (a) UV−visible absorption spectra of **8** in acetonitrile at 25 °C before irradiation (BI, black line) and at the *cis*-rich PSS under 430 (430_{PSS}; red line) and at *trans*-rich PSS under 525 nm irradiation (525_{PSS}; blue line), intermediate PSSs at 450 and 470 nm are added (450_{PSS} and 470_{PSS}; green and yellow lines, respectively). (b) Thermal back-isomerization of compound **8** in acetonitrile at 25 °C: spectra before irradiation (BI), at *cis*-rich PSS (430_{PSS}, 0 hr), and at the *trans*-rich state after thermal relaxation (c) Linear fit of absorbance change at 401 nm over time for compound **8** at 25 °C showing the rate constant *k* (= slope) and $t_{½}$ = 2.7minutes.

The absorption spectra showed strong bands (λ_{max} = 332–429 nm) corresponding to π-π* transitions. Some photoswitches had λ_{max} values in the visible light range, making them suitable for visible light activation. The experimental λ_{max} values exhibited variability across these compounds, influenced by the specific types of heteroaryl moieties present in their structures. For instance, compound **6**, which contains two thiazole moieties, exhibits a λ_{max} value of 429 nm, while compound **8**, which incorporates both thiazole and isothiazole moieties, shows a λ_{max} value of 399 nm. In contrast, compound **4**, which contains two thiadiazole moieties, has a λ_{max} value of 362 nm. This variation highlights how the choice of specific heteroaryl groups influences the absorption properties, with compounds like **6** and **8** absorbing within the visible light range, while others, such as compound **4**, display absorption maxima in the near-UV region. Such differences underscore the important role that the selection of heteroaryl moieties plays in fine-tuning the optical characteristics of photoswitches. This variation aligns closely with the predictions from DFT calculations, indicating that the nature of the heteroaryl substituents plays a crucial role in determining the absorption properties. Figure 45b demonstrates the correlation between calculated and experimental λ_{max} values for compounds **1**-**8**. This analysis reveals a clear positive correlation between calculated and experimental values, with the smallest calculated λ_{max} corresponding to the smallest experimental λ_{max}, and similarly for the largest values. For example, compounds **1** and **2** exhibit smaller calculated λ_{max} values of 377 nm and 366 nm, respectively, which closely correspond to their experimental values of 332 nm and 334

nm. Conversely, compounds **6** and **8** have larger calculated λ_{max} values of 459 nm and 431 nm, which align well with the experimental values of 429 nm and 399 nm. These observations indicate that the methodology employed for calculating the λ_{max} values demonstrates a consistent trend across the various compounds, thereby validating its reliability in theoretical predictions.

The photoswitches demonstrated efficient photoisomerization under light irradiation at appropriate wavelengths, with significant composition shifts between trans-rich and *cis*-rich

(a)

Photo-switches	(π-π^*) (*E*)	(π-π^*) (*E*)	(n-π^*) (*E*)	(n-π^*) (*Z*)	Conversion (%)		$t_{1/2}$
	λ_{max} cal.	λ_{max}	λ_{max}	λ_{max}	*E*–*Z*	*Z*–*E*	(h, 25 °C)
1	377	332	448	448	94 (365 nm)	61 (430 nm)	45.2
2	366	334	448	448	90 (365 nm)	87 (430 nm)	29.4
3	377	345	453	458	93 (365 nm)	74 (430 nm)	24.3
4	404	362	483	484	>58 (405 nm)	>95 (525 nm)	-
5	427	343	450	450	>70 (365 nm)	>77 (470 nm)	3 min
6	459	429	-	535	>70 (430 nm)	>93 (568 nm)	-
7	404	338	463	460	81 (405 nm)	74 (470 nm)	2.9
8	431	399	-	-	>73 (430 nm) >66 (450 nm) >47 (470 nm)	>83 (525 nm)	2.7 min

(b)

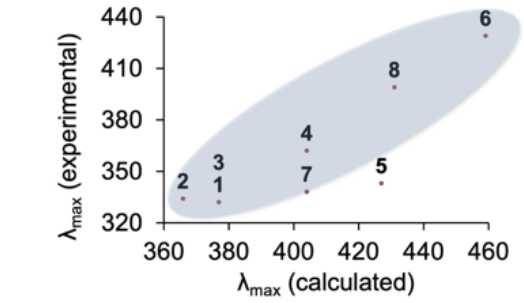

Figure 45: (a) Selected photophysical parameters of photoswitches **1**–**8**. (b) Relationship between experimental and calculated λ_{max}. A grey shadow indicates a positive correlation between them.

photostationary states (PSSs). Photoisomerization studies revealed that compounds **1**, **2**, **3**, and **5** undergo *trans*-to-*cis* isomerization under UV light, achieving high *cis*-isomer compositions at PSS. Specifically, compounds **1**, **2**, and **3** exhibited >90% *cis* isomer at PSS, while compound **5** reached >70% *cis*. The reverse isomerization of these compounds was effectively induced using visible light at 430 nm and 470 nm.

In contrast, compounds **4**, **6**, **7**, and **8** demonstrated reversible photoisomerization using visible light alone. Notably, compounds **7** and **8**, containing the isothiazole group, displayed efficient photoisomerization under longer-wavelength visible light with pronounced composition shifts between *trans*-rich and *cis*-rich PSSs. For instance, compound **7** achieved 81% *cis* isomer at PSS under 405 nm light and reverted to 74% *trans* isomer at PSS under 470 nm light. Compound **8** achieved >73% *cis* isomer at PSS with 430 nm light, >66% *cis* with 450 nm light, and >47% *cis* with 470 nm light. Additionally, under 525 nm light, compound **8** reverted efficiently to its *trans* form, achieving >83% *trans* isomer at PSS (Figure 45a).

The thermal stability ($t_{1/2}$) of *cis* isomers vary from several seconds to tens of hours. Compound **1** showed the longest half-life ($t_{1/2}$ = 45.2 h) among the 8 compounds studied. Compounds **4** and **6** exhibited relatively short half-lives of their *cis*-isomers, so brief that their changes could not be accurately tracked by a conventional spectrophotometer. It was estimated that they have half-lives of approximately several seconds. Compound **7** and **8** showed half-lives of 2.9 hours (λ_{max} = 338 nm) and 2.7 min (λ_{max} = 399 nm), respectively. A general trend was observed in which the

thermal lifetime of the *cis* isomer decreased as the absorption maxima increased. This behavior is similar to that seen in substituted azobenzenes, such as 4-aminoazobenzene,[29] where increased absorption at longer wavelengths corresponds to reduced thermal stability of the *cis* isomer.

3.4 Structural aspects of photoswitches in *trans* and *cis* isomers

Single-crystal X-ray diffraction analysis was performed to better understand the molecular structures of the photoswitches. The analysis revealed that the *trans* isomers of compounds **2**, **3**, **4**, **5**, **6**, and **8** adopt a planar geometry, similar to the well-known azobenzene structure.[30, 31]

In these compounds, the phenyl, azo, and heteroaryl moieties are arranged in a co-planar fashion, with all the involved aromatic rings and the azo linkage lying within the same plane. (Figure 46a-f). In the case of the *cis* isomers, compound **2**, which contains a 1,3,4-thiadiazole ring, exhibits the typically observed twisted geometry found in the *cis* isomer of azobenzene, with the phenyl and thiadiazole rings adopting a face-to-face orientation.

In contrast, the *cis* isomer of compound **3**, which incorporates a 1,2,3-thiadiazole group, displayed an orthogonal geometry. Here, the phenyl and thiadiazole rings are oriented perpendicularly, with the sulfur atom of the thiadiazole ring facing the phenyl ring (Figure 46g). This configuration is similar to that observed in our previously reported phenylazothiazole photoswitch.[18]

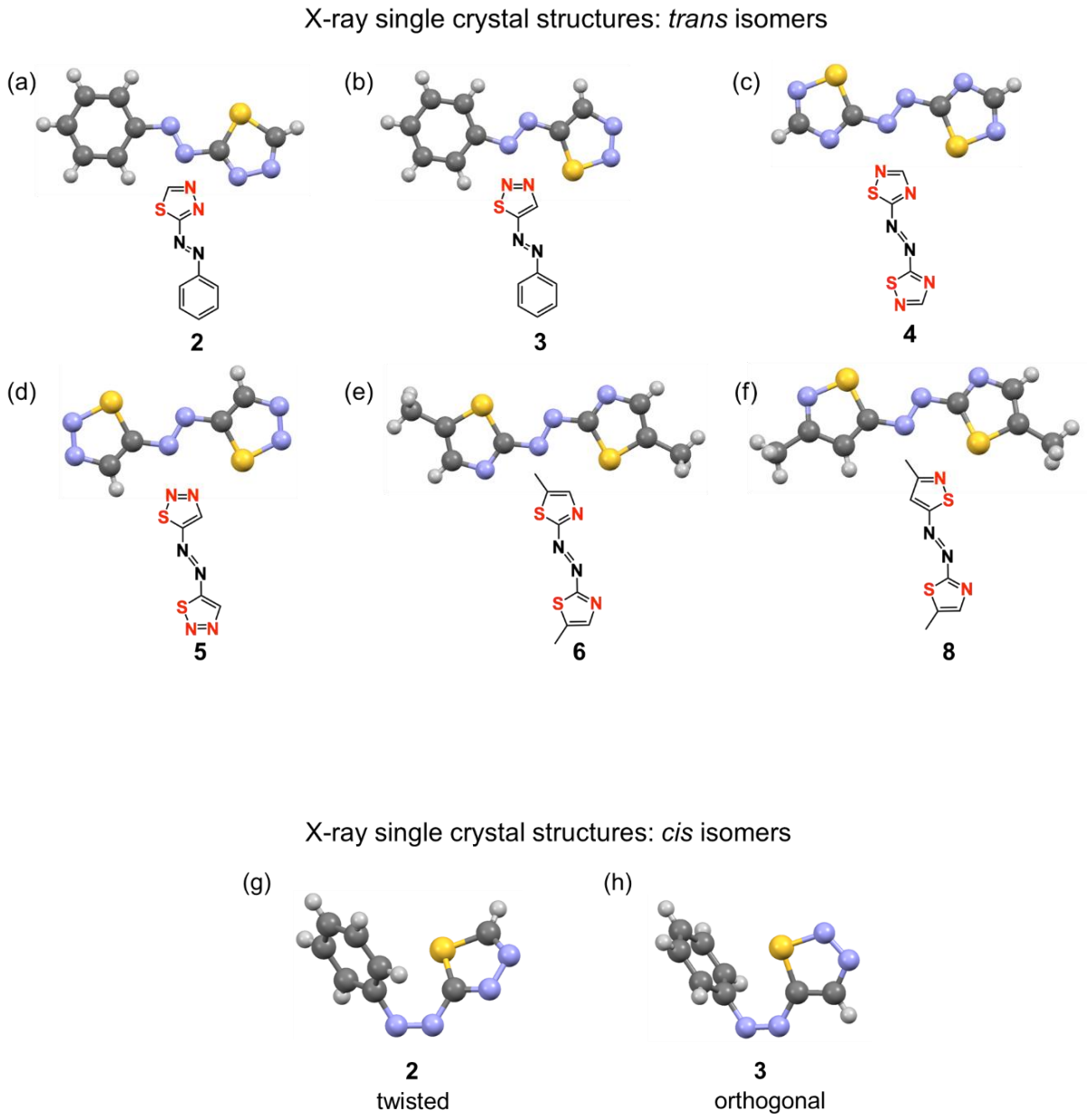

Figure 46: (a-f) Single-crystal X-ray structures of both *trans* isomers of **2**, **3**, **4**, **5**, **6** and **8**, (g-h) *cis* isomers of **2** and **3**. (gray = C; light gray = H; purple = N; gold = S).

Additionally, time-dependent density-functional theory (TDDFT) calculations were carried out in acetonitrile medium to analyse the molecular structure (Figure 47 a-d). The *trans* isomers of compounds **2**–**5** showed planar geometries with phenyl, azo and thiadiazole moieties in the same plane. The *cis* isomers of compounds adopted twisted and orthogonal conformations as seen in the X-ray crystal structure of compound **2** and **3**, respectively. The theoretical calculations of molecular structures match the X-ray crystallography results, confirming their reliability in predicting the molecular geometry of the designed molecules.

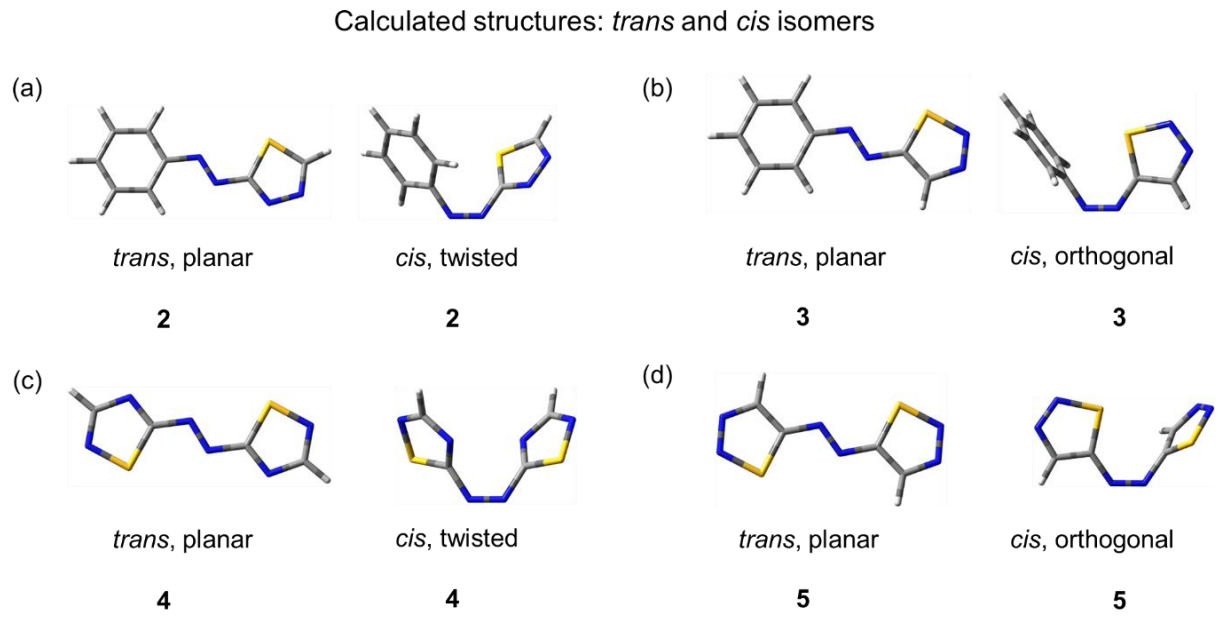

Figure 47: (a–d) Geometry optimized calculated conformations of both *trans* and *cis* isomers of **2**–**5**. (gray = C; light gray = H; purple = N; gold = S).

4. Conclusion

In conclusion, I have synthesized novel azophotoswitches with various five-membered heteroaryl groups such as thiazole, isothiazole, thiadiazole and isothiadiazole. These compounds were designed with heteroaryl units on either one or both sides of the azo bond. DFT calculations were used to predict the λmax values of 24 compounds, resulting in the selection of eight compounds for study, including those with the longest λmax. Compound 8 containing thiazole and isothiazole moieties, showed longer λmax than any of the synthesized compounds. The λmax of the photoswitch shifted to longer wavelength with decrease in cis-life time, as seen in substituted azobenzenes. It efficiently isomerized under visible light at 430 nm, 450 nm, 470 nm (trans – cis) and 525 nm (cis – trans). X-ray crystallography showed that the trans isomers displayed a planar geometry, while the cis isomer of compound 3 adopted a unique orthogonal conformation. The calculations employed in the study reliably predicted both the absorbance maximum and molecular geometry. This work will expand the range of visible-light active photoswitches design, facilitating advancements in photopharmacology.

5. Time-dependent density-functional theory (TDDFT) calculations coordinates

Table S1. Cartesian coordinates of ground state optimized geometry of **a**.

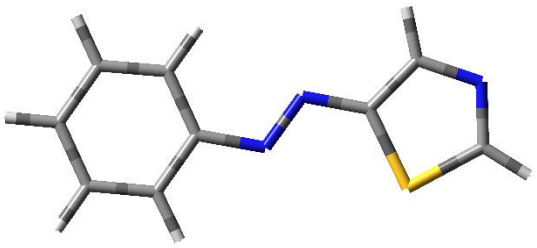

	X	Y	Z
S	2.554615	-1.18844	-5.9E-05
N	-0.3112	-0.37116	0.000087
N	0.432275	0.652256	-4E-06
C	-1.70246	-0.12225	0.000042
C	-2.29075	1.158604	-0.0001
H	-1.65894	2.039248	-0.00018
C	1.784937	0.401652	-1.7E-05
C	-2.51435	-1.26845	0.000152
H	-2.04023	-2.24505	0.00026
C	-4.48826	0.12855	-0.00002
H	-5.56927	0.230367	-4.4E-05
C	-3.6775	1.274684	-0.00013
H	-4.1343	2.259826	-0.00024
C	-3.90439	-1.14201	0.000121
H	-4.52847	-2.03018	0.000207
C	4.089457	-0.36731	0.000278
H	5.010867	-0.93845	0.000331
C	2.753899	1.383782	-0.00016
N	4.051476	0.943388	-0.0001
H	2.535116	2.444355	-0.00027

Table S2. Cartesian coordinates of ground state optimized geometry of **b**.

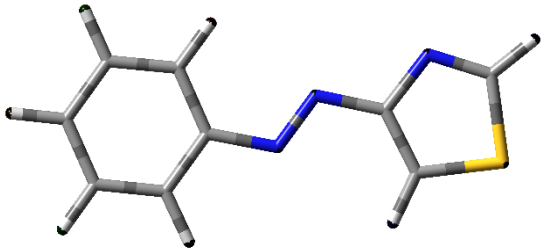

	X	Y	Z
N	-0.43435	-0.43417	0.000029
N	0.315021	0.57959	-3.6E-05
C	-1.82525	-0.16795	0.000046
C	-2.39895	1.119084	-2E-06
H	-1.75639	1.991863	-5.7E-05
C	-2.64976	-1.3044	0.000117
H	-2.18634	-2.28616	0.000154
C	-4.60805	0.11402	0.000093
H	-5.68787	0.22812	0.000111
C	-3.78432	1.251019	0.000022
H	-4.23015	2.241217	-1.5E-05
C	-4.03876	-1.16287	0.000141
H	-4.67272	-2.04405	0.000196
C	1.690047	0.292469	-4.5E-05
C	2.310173	-0.94041	0.000058
N	2.538712	1.383404	-0.00014
S	4.016505	-0.73648	-0.00012
C	3.781398	0.998128	-1.8E-05
H	4.630408	1.670823	-6.8E-05
H	1.844191	-1.91455	0.00015

Table S3. Cartesian coordinates of ground state optimized geometry of **c**.

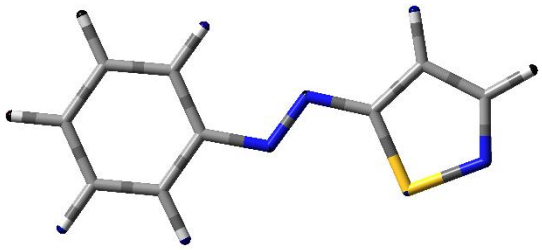

	X	Y	Z
S	-2.52244	-1.15989	-0.00065
N	0.304797	-0.32542	0
N	-0.42673	0.706157	0.000119
C	1.696832	-0.10061	0.000046
C	2.305625	1.171334	0.000226
H	1.688179	2.062024	0.000342
C	-1.78596	0.434333	0.000039
C	2.487596	-1.2621	-0.0001
H	1.995474	-2.22962	-0.00024
C	4.483227	0.101516	0.000106
H	5.565789	0.184887	0.000131
C	3.69337	1.262823	0.000252
H	4.168318	2.239182	0.00039
C	3.879127	-1.15955	-0.00007
H	4.488619	-2.05758	-0.00018
C	-2.77716	1.393175	-7.6E-05
H	-2.58978	2.45914	-0.00011
C	-4.05856	0.779118	0.000271
H	-4.99987	1.319906	0.000566
N	-4.09268	-0.54358	0.000642

Table S4. Cartesian coordinates of ground state optimized geometry of **d**.

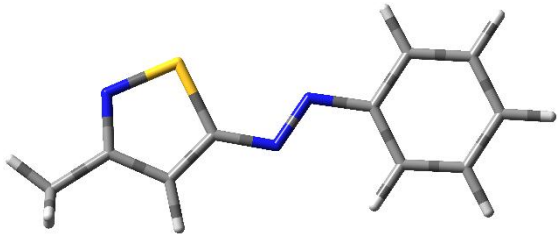

	X	Y	Z
S	-2.01475	-1.4323	0.000097
N	0.752877	-0.40602	-9.9E-05
N	-0.04842	0.572155	-0.00017
C	2.126221	-0.08279	-3.5E-05
C	2.642099	1.229345	0.000089
H	1.961756	2.072971	0.000144
C	-1.38626	0.208217	-8.4E-05
C	2.99856	-1.18414	-9.1E-05
H	2.577706	-2.18473	-0.00018
C	4.891219	0.319709	0.000078
H	5.964974	0.480708	0.000123
C	4.019709	1.420902	0.000146
H	4.4229	2.429011	0.000247
C	4.379249	-0.98145	-4.3E-05
H	5.051661	-1.83344	-9.5E-05
C	-2.43704	1.096151	-0.00019
H	-2.31677	2.172201	-0.00036
C	-3.69083	0.409739	-4.7E-05
N	-3.62296	-0.91342	0.000091
C	-5.02661	1.094845	0.000072
H	-5.13122	1.733314	0.88393
H	-5.13031	1.735548	-0.88225
H	-5.83319	0.359047	-0.0012

Table S5. Cartesian coordinates of ground state optimized geometry of **e**.

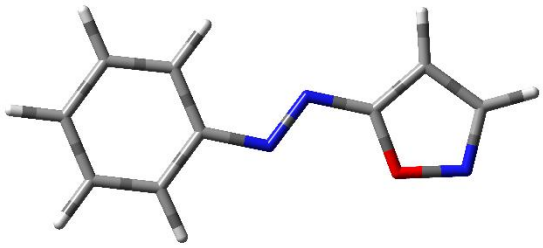

	X	Y	Z
N	0.044854	-0.44654	0.000084
N	-0.71982	0.562153	0.000118
C	-2.07197	0.273105	0.00004
O	-2.54906	-0.99853	-6.4E-05
C	-4.2633	0.330802	-1.9E-05
H	-5.30733	0.616194	-2.9E-05
N	-3.94986	-0.94848	-0.00012
C	-3.11545	1.162932	0.000051
H	-3.05724	2.239918	0.000121
C	1.425954	-0.16013	0.000031
C	2.265424	-1.28725	0.000051
C	1.980421	1.136708	-3.5E-05
C	3.651267	-1.12591	0.000013
H	1.814582	-2.27463	0.0001
C	3.362823	1.286971	-7.9E-05
H	1.325893	2.000472	-5.5E-05
C	4.200931	0.159805	-5.5E-05
H	4.298368	-1.99721	0.000033
H	3.7964	2.282334	-0.00013
H	5.278987	0.289005	-8.9E-05

Table S6. Cartesian coordinates of ground state optimized geometry of **f**.

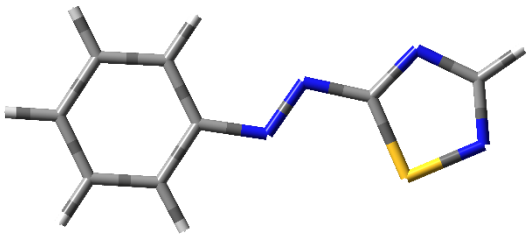

	X	Y	Z
S	2.508362	-1.15728	-1E-06
N	-0.28184	-0.28987	0.000055
N	0.441723	0.747213	0.000004
N	2.716265	1.396346	-0.00008
C	-1.67037	-0.08523	0.000032
C	-2.29487	1.180731	-0.00005
H	-1.68872	2.079063	-0.0001
C	1.802747	0.451984	-1.7E-05
C	-2.44341	-1.26022	0.000099
H	-1.9363	-2.21974	0.000162
C	3.950738	0.809411	-6.3E-05
H	4.843428	1.424903	-0.0001
C	-4.45421	0.077535	0.000006
H	-5.53775	0.146196	-5E-06
C	-3.68225	1.251936	-6.3E-05
H	-4.17254	2.220377	-0.00013
C	-3.83518	-1.17649	0.000087
H	-4.43364	-2.08159	0.00014
N	4.059931	-0.5038	0.000002

Table S7. Cartesian coordinates of ground state optimized geometry of **g**.

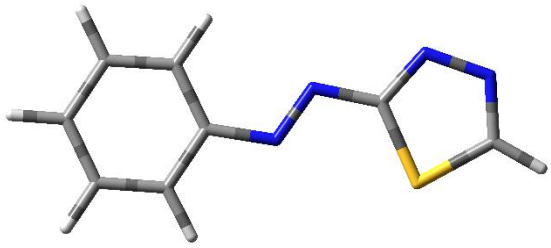

	X	Y	Z
S	2.522988	-1.1818	0.000097
N	-0.28442	-0.32098	0.000044
N	0.4454	0.709525	-0.00002
N	2.684387	1.405165	-7.3E-05
C	-1.67433	-0.10031	-8E-06
C	-2.28514	1.171272	-0.00013
H	-1.66975	2.063366	-0.00019
C	1.80602	0.43082	0.000004
C	-2.46015	-1.2657	0.00007
H	-1.96422	-2.23112	0.000161
C	-4.45763	0.093175	-8.7E-05
H	-5.54037	0.173589	-0.00012
C	-3.67231	1.258138	-0.00017
H	-4.15111	2.232407	-0.00026
C	-3.85145	-1.16696	0.000031
H	-4.45915	-2.06599	0.000091
C	4.045178	-0.3544	0.000114
H	4.988366	-0.88729	0.000177
N	3.972816	0.953094	-0.00001

Table S8. Cartesian coordinates of ground state optimized geometry of **h**.

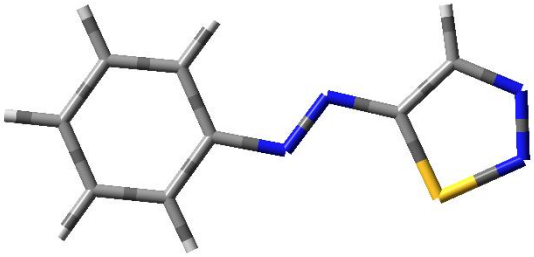

	X	Y	Z
S	-2.55314	-1.165	-0.00034
N	0.306049	-0.34703	-1.5E-05
N	-0.4353	0.678352	0.000073
C	1.69315	-0.11008	0.000036
C	2.290698	1.168009	0.000155
H	1.665882	2.053471	0.000217
C	-1.7902	0.394191	0.000011
C	2.492553	-1.26653	-4.6E-05
H	2.00753	-2.2375	-0.00014
C	4.47534	0.11407	0.00011
H	5.55714	0.20629	0.00014
C	3.676935	1.270077	0.00019
H	4.144886	2.24964	0.000281
C	3.882642	-1.15252	-8E-06
H	4.500008	-2.04499	-6.9E-05
N	-4.04743	0.857923	0.000038
C	-2.77943	1.359399	0.00004
H	-2.61342	2.428253	0.00012
N	-4.11789	-0.4285	0.000181

Table S9. Cartesian coordinates of ground state optimized geometry of **i**.

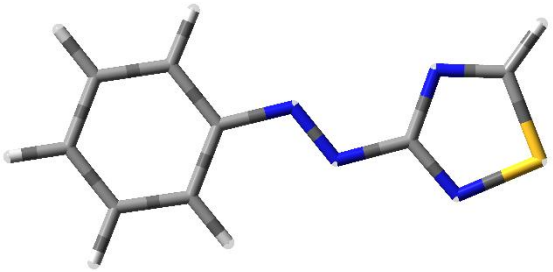

	X	Y	Z
N	-0.44461	0.512397	-0.00022
N	0.348842	-0.46608	-0.00016
C	-1.81851	0.178733	-5.2E-05
C	-2.32773	-1.13575	0.000202
H	-1.64294	-1.97568	0.000284
C	-2.69512	1.27611	-0.00016
H	-2.27808	2.278278	-0.00036
C	-4.5803	-0.23605	0.000227
H	-5.65333	-0.40207	0.000335
C	-3.70425	-1.33382	0.00034
H	-4.10342	-2.3435	0.000536
C	-4.0751	1.067591	-2.6E-05
H	-4.75164	1.916251	-0.00011
C	1.710049	-0.11057	-0.00011
S	4.110682	-0.46753	-0.00014
C	3.482801	1.152716	0.000116
H	4.118646	2.030883	0.000175
N	2.5721	-1.11495	0.000023
N	2.179211	1.186147	0.000094

Table S10. Cartesian coordinates of ground state optimized geometry of **j**.

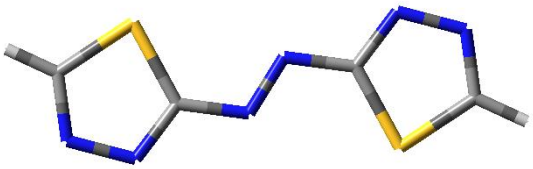

	X	Y	Z
S	-2.55404	1.189004	-0.00027
N	0.334216	0.535207	-0.00015
N	-0.33421	-0.53518	-0.00012
N	-2.50186	-1.40206	-0.00015
C	-1.70846	-0.35415	-0.00015
C	-3.99794	0.239687	-0.00025
H	-4.98218	0.69219	-0.00031
N	-3.81637	-1.06117	-0.00022
C	1.70846	0.354139	0.000075
S	2.553955	-1.18896	0.00034
N	2.501957	1.402026	0.000039
C	3.997905	-0.23974	0.000463
N	3.81648	1.061136	0.000256
H	4.982097	-0.69233	0.000647

Table S11. Cartesian coordinates of ground state optimized geometry of **k**.

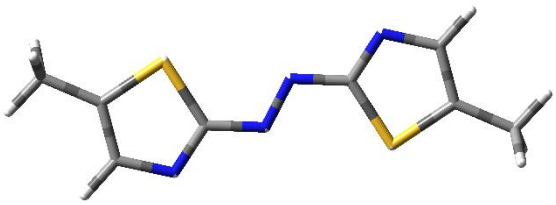

	X	Y	Z
S	-2.62123	0.975518	-0.00009
N	0.289711	0.5656	-2.2E-05
N	-0.28971	-0.56561	-2.3E-05
N	-2.38138	-1.62148	-6.6E-05
C	-1.66537	-0.51805	-0.00003
C	-3.71455	-1.33391	-0.00004
H	-4.43598	-2.14281	-4.2E-05
C	-4.06319	0.001637	0.000034
C	1.665366	0.518041	0.00003
S	2.621233	-0.97552	0.000135
N	2.381374	1.621474	0.000044
C	4.063185	-0.00164	-5.6E-05
C	3.714542	1.333907	0.000039
H	4.435971	2.142814	0.000014
C	-5.4372	0.591403	0.000107
H	-5.60237	1.216833	0.88387
H	-5.60243	1.216914	-0.88359
H	-6.1811	-0.20927	0.000096
C	5.437205	-0.59139	-0.00012
H	5.602489	-1.21673	0.883688
H	5.602321	-1.217	-0.88377
H	6.181096	0.209283	-0.00031

Table S12. Cartesian coordinates of ground state optimized geometry of **l**.

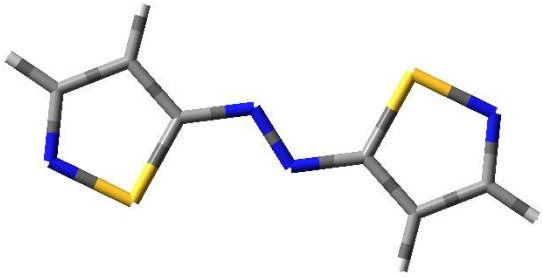

	X	Y	Z
S	2.560874	1.173354	-0.0005
N	-0.3371	0.537376	-5.7E-05
N	0.337274	-0.53743	0.000095
C	1.707072	-0.36015	0
C	2.622731	-1.39377	0.000035
H	2.353489	-2.44201	0.000158
N	4.075381	0.439538	-7E-06
C	3.94538	-0.878	0.000039
H	4.844412	-1.48576	0.000183
C	-1.70679	0.359821	0.000103
S	-2.56142	-1.17368	0.000046
C	-2.62218	1.39377	-4.8E-05
N	-4.07561	-0.43895	0.000606
H	-2.35266	2.441939	-0.00025
C	-3.94497	0.878434	0.00027
H	-4.84366	1.486712	0.000369

Table S13. Cartesian coordinates of ground state optimized geometry of **m**.

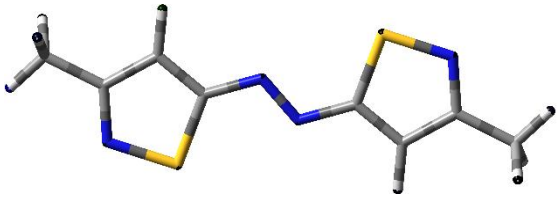

	X	Y	Z
S	-2.37216	-1.52057	-9.9E-05
N	0.408542	-0.48534	-0.00029
N	-0.40854	0.48532	-0.00018
C	-1.7406	0.118031	-0.00015
C	-2.78974	1.010548	0.000023
H	-2.66569	2.086103	0.000135
N	-3.975	-0.99731	-0.00044
C	-4.04368	0.326813	-0.00015
C	1.740604	-0.11804	-2.1E-05
S	2.372145	1.520566	0.00061
C	2.789746	-1.01055	0.000003
N	3.974995	0.997315	0.000157
H	2.66571	-2.08611	-0.0002
C	4.043684	-0.32681	0.000104
C	-5.37928	1.011205	-0.00017
H	-5.48336	1.65002	0.883296
H	-5.48292	1.650863	-0.88306
H	-6.18521	0.274936	-0.00071
C	5.379287	-1.01119	-2.1E-05
H	5.483344	-1.65019	0.883307
H	5.482951	-1.65066	-0.88305
H	6.185217	-0.27492	-0.00038

Table S14. Cartesian coordinates of ground state optimized geometry of **n**.

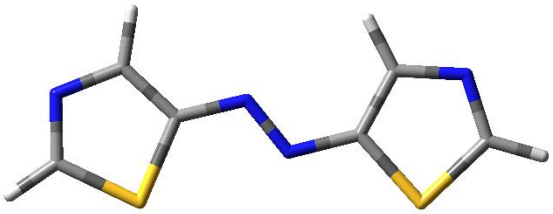

	X	Y	Z
S	-2.47329	-1.18903	-0.00021
N	0.351124	-0.23751	0.000021
N	-0.44478	0.753582	0.000057
C	-1.77928	0.435369	-4.1E-05
C	-4.0441	-0.44055	-0.0002
H	-4.93788	-1.05397	-0.00029
C	-2.7949	1.372304	-3.4E-05
N	-4.06824	0.871193	-0.00013
H	-2.62524	2.441947	0.000049
C	1.695472	0.096599	0.000094
S	2.864979	-1.20555	-1.4E-05
C	2.357504	1.31306	0.000215
C	4.123325	-0.01326	0.000234
N	3.721876	1.238335	0.00029
H	1.863039	2.27542	0.000276
H	5.165096	-0.31058	0.000271

Table S15. Cartesian coordinates of ground state optimized geometry of **o**.

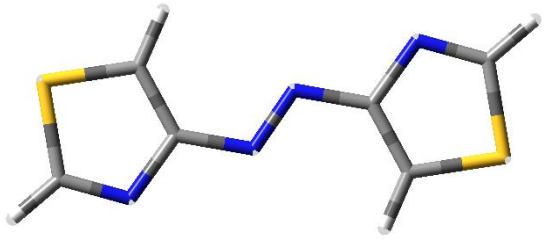

	X	Y	Z
N	-0.35869	-0.51935	0.00007
N	0.358721	0.519217	0
C	1.740259	0.278498	-4.5E-05
C	2.401203	-0.93383	-6.2E-05
N	2.551234	1.397581	-0.00018
S	4.098692	-0.67271	0.000149
C	3.805651	1.053778	-0.00033
H	4.632175	1.753924	-0.00044
H	1.967736	-1.92298	-3E-06
C	-1.74031	-0.27853	0.000029
C	-2.40124	0.933691	-0.00013
N	-2.55125	-1.39775	0.000063
S	-4.09868	0.672827	0.000157
H	-1.96768	1.922818	-0.00021
C	-3.80561	-1.0536	-0.00011
H	-4.63219	-1.75365	-0.00011

Table S16. Cartesian coordinates of ground state optimized geometry of **p**.

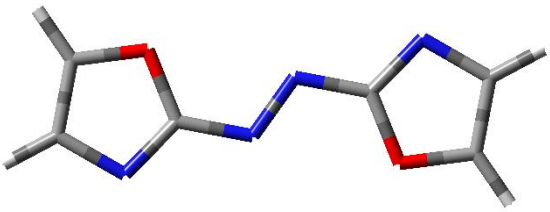

	X	Y	Z
N	0.369823	0.517108	0.000017
N	-0.36998	-0.5174	0.00009
C	1.718511	0.262581	0.000142
C	3.580285	-0.82896	0.000393
C	3.833326	0.515148	0.000295
H	4.191897	-1.71742	0.000543
H	4.787911	1.019499	0.000334
O	2.229697	-1.0039	0.000311
N	2.63865	1.198681	0.00006
C	-1.71855	-0.26267	-0.00011
O	-2.22954	1.003894	-0.00036
N	-2.63878	-1.19869	-7.5E-05
C	-3.58017	0.829127	-0.00048
C	-3.83332	-0.51496	-0.00028
H	-4.19165	1.717674	-0.00068
H	-4.78795	-1.01921	-0.00029

Table S17. Cartesian coordinates of ground state optimized geometry of **q**.

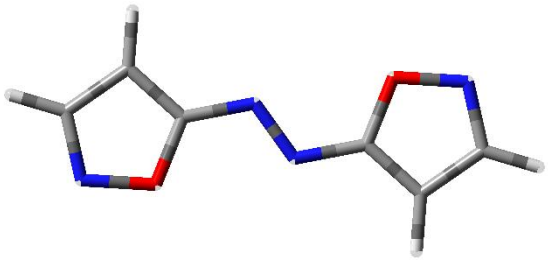

	X	Y	Z
N	-0.37091	0.515662	-4.8E-05
N	0.370841	-0.51547	-0.00013
C	-1.72418	0.25702	-0.00015
C	-3.91231	0.36622	-0.00014
H	-4.94974	0.673814	-0.0001
O	-2.22931	-1.00369	-0.00028
C	1.72413	-0.25695	0.000082
O	2.229423	1.003694	0.000371
C	3.91231	-0.36636	0.000422
H	4.949713	-0.67406	0.000546
N	-3.62461	-0.91962	-0.00047
N	3.624723	0.919492	0.000438
C	-2.74634	1.172314	-0.00016
H	-2.66258	2.247667	-0.00007
C	2.746229	-1.17231	0.000026
H	2.662365	-2.24765	-0.00018

Table S18. Cartesian coordinates of ground state optimized geometry of **r**.

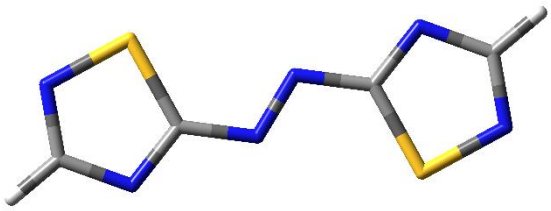

	X	Y	Z
S	-2.56218	1.167643	0.000343
N	0.326497	0.540181	-0.00019
N	-0.32645	-0.53996	-0.00025
N	-2.52164	-1.39368	0.000015
C	-1.70634	-0.36181	-0.00017
C	-3.80353	-0.93123	-8.7E-05
H	-4.63541	-1.62587	-0.00034
N	-4.03335	0.370463	-0.00049
C	1.706401	0.361802	-0.0001
S	2.562047	-1.16762	0.000307
N	2.521766	1.393652	0.000191
N	4.033262	-0.37059	-0.00046
C	3.803671	0.931122	0.000065
H	4.635626	1.625682	-0.00012

Table S19. Cartesian coordinates of ground state optimized geometry of **s**.

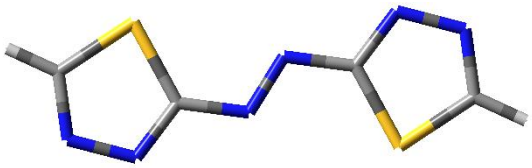

	X	Y	Z
S	-2.55404	1.189004	-0.00027
N	0.334216	0.535207	-0.00015
N	-0.33421	-0.53518	-0.00012
N	-2.50186	-1.40206	-0.00015
C	-1.70846	-0.35415	-0.00015
C	-3.99794	0.239687	-0.00025
H	-4.98218	0.69219	-0.00031
N	-3.81637	-1.06117	-0.00022
C	1.70846	0.354139	0.000075
S	2.553955	-1.18896	0.00034
N	2.501957	1.402026	0.000039
C	3.997905	-0.23974	0.000463
N	3.81648	1.061136	0.000256
H	4.982097	-0.69233	0.000647

Table S20. Cartesian coordinates of ground state optimized geometry of **t**.

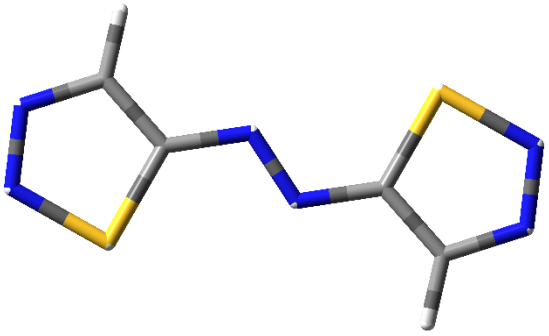

	X	Y	Z
S	2.580183	1.175195	-0.0003
N	-0.3468	0.52968	-8.6E-05
N	0.347091	-0.53046	0.000019
C	1.712995	-0.32648	-6.2E-05
N	3.929108	-0.94831	-8.8E-05
C	2.631079	-1.36143	0.000019
H	2.389793	-2.41587	0.000152
N	4.08383	0.33146	-0.00022
C	-1.71279	0.326071	0.000041
S	-2.58096	-1.17519	0.000298
C	-2.63033	1.361405	-4.8E-05
N	-4.08378	-0.33091	0.000327
N	-3.92866	0.948894	0.000105
H	-2.38867	2.415773	-0.00022

Table S21. Cartesian coordinates of ground state optimized geometry of **u**.

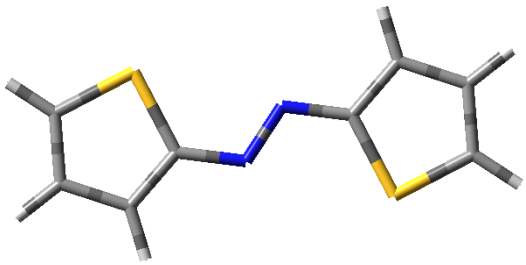

	X	Y	Z
N	0.348462	0.533463	0.000524
N	-0.3482	-0.53252	0.000508
C	1.710321	0.362381	0.000342
S	2.536443	-1.20454	-9.1E-05
C	4.076382	-0.40263	0.000509
C	3.966779	0.967972	0.000293
H	4.984012	-0.99236	0.000692
H	4.821889	1.633202	0.00036
C	2.616922	1.408466	0.0002
H	2.300937	2.444777	0.000214
C	-1.71006	-0.36201	0.000132
S	-2.53708	1.204605	-0.00081
C	-2.61634	-1.40841	-9.3E-05
C	-4.07655	0.40192	-0.00013
C	-3.96632	-0.96864	-0.00022
H	-2.29982	-2.44457	0.000075
H	-4.9844	0.991308	-0.00012
H	-4.82112	-1.63428	-0.00019

Table S22. Cartesian coordinates of ground state optimized geometry of **v**.

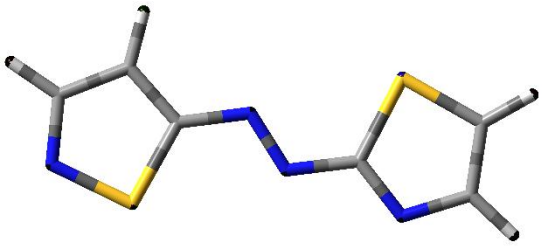

	X	Y	Z
N	-0.32266	0.532553	0.000011
N	0.351315	-0.54203	0.000016
C	-1.69173	0.357829	-0.0001
S	-2.54934	-1.17379	-0.00028
C	1.72241	-0.37255	0.000123
S	2.540774	1.19769	0.000177
C	4.042006	0.34869	0.000433
C	3.833924	-1.01185	0.000255
H	4.986107	0.876865	0.000601
H	4.62189	-1.75461	0.00029
C	-2.60585	1.393302	-0.00015
H	-2.33417	2.440867	-9.9E-05
N	-4.06298	-0.4371	-0.00025
N	2.528842	-1.41199	0.000094
C	-3.92936	0.880251	-0.00023
H	-4.82681	1.490425	-0.00024

Table S23. Cartesian coordinates of ground state optimized geometry of **w**.

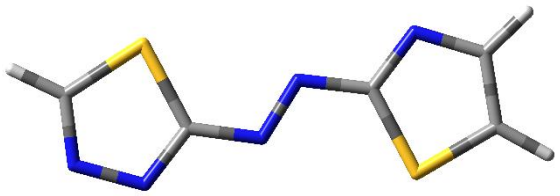

	X	Y	Z
S	2.530865	-1.19511	-0.00013
N	-0.34254	-0.54651	0.00008
N	0.328161	0.527199	0.000069
N	2.494247	1.415094	-5.7E-05
C	1.697776	0.36592	-3.5E-05
C	4.020173	-0.3327	-0.00024
H	4.969535	-0.85158	-0.00034
C	-1.71423	-0.36074	0.000155
S	-2.54778	1.192455	-0.00012
N	-2.51891	-1.39965	-0.00011
C	-4.00276	0.255595	0.000754
N	-3.83304	-1.04477	0.000127
H	-4.9827	0.717308	0.00093
C	3.800059	1.028575	-0.00018
H	4.582268	1.777261	-0.00022

Table S24. Cartesian coordinates of ground state optimized geometry of **x**.

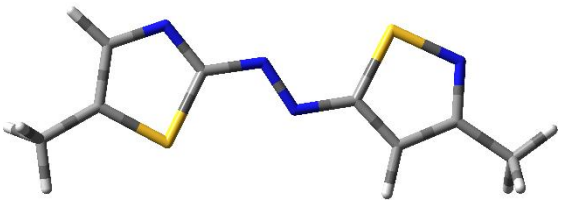

	X	Y	Z
S	-2.50512	-1.05252	-0.00041
N	0.349663	-0.32756	0.000114
N	-0.35371	0.730617	0.000069
C	-1.71544	0.532099	-5.7E-05
C	-3.84021	1.123837	-8.3E-05
C	1.712893	-0.11182	0.000089
S	2.523322	1.447355	-0.00012
C	2.658563	-1.11401	0.000092
N	4.060351	0.75032	0.000182
H	2.417696	-2.16962	0.00012
C	3.980151	-0.57302	0.000157
C	5.231295	-1.40259	0.000333
H	5.263068	-2.04912	0.883851
H	5.262848	-2.04986	-0.88264
H	6.114464	-0.7609	-2.9E-05
C	-4.04126	-0.24448	0.000088
N	-2.54864	1.55227	-0.00042
H	-4.64449	1.850487	0.000019
C	-5.34879	-0.97734	0.000399
H	-5.93469	-0.70698	0.885222
H	-5.93531	-0.70657	-0.88389
H	-5.21168	-2.0604	0.000104

6. References

(1) Goulet-Hanssens, A.; Eisenreich, F.; Hecht, S. Enlightening Materials with Photoswitches. *Advanced Materials* **2020**, *32* (20), 1905966. https://doi.org/10.1002/adma.201905966.

(2) *Molecular Photoswitches: Chemistry, Properties, and Applications, 2 Volume Set | Wiley*. Wiley.com. https://www.wiley.com/en-jp/Molecular+Photoswitches%3A+Chemistry%2C+Properties%2C+and+Applications%2C+2+Volume+Set-p-9783527347681 (accessed 2024-10-01).

(3) Mukherjee, A.; Seyfried, M. D.; Ravoo, B. J. Azoheteroarene and Diazocine Molecular Photoswitches: Self-Assembly, Responsive Materials and Photopharmacology. *Angewandte Chemie International Edition* **2023**, *62* (42), e202304437. https://doi.org/10.1002/anie.202304437.

(4) Kobauri, P.; Dekker, F. J.; Szymanski, W.; Feringa, B. L. Rational Design in Photopharmacology with Molecular Photoswitches. *Angewandte Chemie International Edition* **2023**, *62* (30), e202300681. https://doi.org/10.1002/anie.202300681.

(5) Sadovski, O.; Beharry, A. A.; Zhang, F.; Woolley, G. A. Spectral Tuning of Azobenzene Photoswitches for Biological Applications. *Angewandte Chemie International Edition* **2009**, *48* (8), 1484–1486. https://doi.org/10.1002/anie.200805013.

(6) Beharry, A. A.; Sadovski, O.; Woolley, G. A. Azobenzene Photoswitching without Ultraviolet Light. *J. Am. Chem. Soc.* **2011**, *133* (49), 19684–19687. https://doi.org/10.1021/ja209239m.

(7) Samanta, S.; Beharry, A. A.; Sadovski, O.; McCormick, T. M.; Babalhavaeji, A.; Tropepe, V.; Woolley, G. A. Photoswitching Azo Compounds in Vivo with Red Light. *J. Am. Chem. Soc.* **2013**, *135* (26), 9777–9784. https://doi.org/10.1021/ja402220t.

(8) Crespi, S.; Simeth, N. A.; König, B. Heteroaryl Azo Dyes as Molecular Photoswitches. *Nat Rev Chem* **2019**, *3* (3), 133–146. https://doi.org/10.1038/s41570-019-0074-6.

(9) Weston, C. E.; Richardson, R. D.; Fuchter, M. J. Photoswitchable Basicity through the Use of Azoheteroarenes. *Chem. Commun.* **2016**, *52* (24), 4521–4524. https://doi.org/10.1039/C5CC10380K.

(10) Devi, S.; Saraswat, M.; Grewal, S.; Venkataramani, S. Evaluation of Substituent Effect in Z-Isomer Stability of Arylazo-1H-3,5-Dimethylpyrazoles: Interplay of Steric, Electronic

Effects and Hydrogen Bonding. *J. Org. Chem.* **2018**, *83* (8), 4307–4322. https://doi.org/10.1021/acs.joc.7b02604.

(11) Gaur, A. K.; Kumar, H.; Gupta, D.; Tom, I. P.; Nampoothiry, D. N.; Thakur, S. K.; Mahadevan, A.; Singh, S.; Venkataramani, S. Structure–Property Relationship for Visible Light Bidirectional Photoswitchable Azoheteroarenes and Thermal Stability of Z-Isomers. *J. Org. Chem.* **2022**, *87* (10), 6541–6551. https://doi.org/10.1021/acs.joc.2c00088.

(12) Otsuki, J.; Suwa, K.; Sarker, K. K.; Sinha, C. Photoisomerization and Thermal Isomerization of Arylazoimidazoles. *J. Phys. Chem. A* **2007**, *111* (8), 1403–1409. https://doi.org/10.1021/jp066816p.

(13) Calbo, J.; Weston, C. E.; White, A. J. P.; Rzepa, H. S.; Contreras-García, J.; Fuchter, M. J. Tuning Azoheteroarene Photoswitch Performance through Heteroaryl Design. *J. Am. Chem. Soc.* **2017**, *139* (3), 1261–1274. https://doi.org/10.1021/jacs.6b11626.

(14) Fang, D.; Zhang, Z.-Y.; Shangguan, Z.; He, Y.; Yu, C.; Li, T. (Hetero)Arylazo-1,2,3-Triazoles: "Clicked" Photoswitches for Versatile Functionalization and Electronic Decoupling. *J. Am. Chem. Soc.* **2021**, *143* (36), 14502–14510. https://doi.org/10.1021/jacs.1c08704.

(15) Slavov, C.; Yang, C.; Heindl, A. H.; Wegner, H. A.; Dreuw, A.; Wachtveitl, J. Thiophenylazobenzene: An Alternative Photoisomerization Controlled by Lone-Pair···π Interaction. *Angewandte Chemie International Edition* **2020**, *59* (1), 380–387. https://doi.org/10.1002/anie.201909739.

(16) Kennedy, A. D. W.; Sandler, I.; Andréasson, J.; Ho, J.; Beves, J. E. Visible-Light Photoswitching by Azobenzazoles. *Chemistry – A European Journal* **2020**, *26* (5), 1103–1110. https://doi.org/10.1002/chem.201904309.

(17) Matsuo, K.; Thayyil, S.; Kawaguchi, M.; Nakagawa, H.; Tamaoki, N. A Visible Light-Controllable Rho Kinase Inhibitor Based on a Photochromic Phenylazothiazole. *Chem. Commun.* **2021**, *57* (93), 12500–12503. https://doi.org/10.1039/D1CC04905D.

(18) Lin, R.; Hashim, P. K.; Sahu, S.; Amrutha, A. S.; Cheruthu, N. M.; Thazhathethil, S.; Takahashi, K.; Nakamura, T.; Kikukawa, T.; Tamaoki, N. Phenylazothiazoles as Visible-Light Photoswitches. *J. Am. Chem. Soc.* **2023**, *145* (16), 9072–9080. https://doi.org/10.1021/jacs.3c00609.

(19) Dang, T.; Dong, D.; Zhang, J.; He, Y.; Zhang, Z.-Y.; Li, T. Thiazolylazopyrazoles as Nonsymmetric Bis-Heteroaryl Azo Switches: High-Yield Visible-Light Photoisomerization and Increased Z-Isomer Stability by o-Carbonylation. *Angewandte Chemie International Edition* **2023**, *62* (24), e202301992. https://doi.org/10.1002/anie.202301992.

(20) *Visible-Light-Activated Heteroaryl Azoswitches: Toward a More Colorful Future | Journal of the American Chemical Society*. https://pubs.acs.org/doi/10.1021/jacs.4c03135 (accessed 2024-12-10).

(21) Weston, C. E.; Richardson, R. D.; Haycock, P. R.; White, A. J. P.; Fuchter, M. J. Arylazopyrazoles: Azoheteroarene Photoswitches Offering Quantitative Isomerization and Long Thermal Half-Lives. *J. Am. Chem. Soc.* **2014**, *136* (34), 11878–11881. https://doi.org/10.1021/ja505444d.

(22) He, Y.; Shangguan, Z.; Zhang, Z.-Y.; Xie, M.; Yu, C.; Li, T. Azobispyrazole Family as Photoswitches Combining (Near-) Quantitative Bidirectional Isomerization and Widely Tunable Thermal Half-Lives from Hours to Years. *Angewandte Chemie International Edition* **2021**, *60* (30), 16539–16546. https://doi.org/10.1002/anie.202103705.

(23) Naim, M. J.; Alam, O.; Nawaz, F.; Alam, M. J.; Alam, P. Current Status of Pyrazole and Its Biological Activities. *Journal of Pharmacy and Bioallied Sciences* **2016**, *8* (1), 2. https://doi.org/10.4103/0975-7406.171694.

(24) Alghamdi, S. S.; Suliman, R. S.; Almutairi, K.; Kahtani, K.; Aljatli, D. <p>Imidazole as a Promising Medicinal Scaffold: Current Status and Future Direction</P>. *DDDT* **2021**, *15*, 3289–3312. https://doi.org/10.2147/DDDT.S307113.

(25) Zhang, S.-W.; Gong, C.-J.; Su, M.-B.; Chen, F.; He, T.; Zhang, Y.-M.; Shen, Q.-Q.; Su, Y.; Ding, J.; Li, J.; Chen, Y.; Nan, F.-J. Synthesis and in Vitro and in Vivo Biological Evaluation of Tissue-Specific Bisthiazole Histone Deacetylase (HDAC) Inhibitors. *J. Med. Chem.* **2020**, *63* (2), 804–815. https://doi.org/10.1021/acs.jmedchem.9b01792.

(26) Chen, F.; Chai, H.; Su, M.-B.; Zhang, Y.-M.; Li, J.; Xie, X.; Nan, F.-J. Potent and Orally Efficacious Bisthiazole-Based Histone Deacetylase Inhibitors. *ACS Med. Chem. Lett.* **2014**, *5* (6), 628–633. https://doi.org/10.1021/ml400470s.

(27) Zhang, H.-Z.; Zhao, Z.-L.; Zhou, C.-H. Recent Advance in Oxazole-Based Medicinal Chemistry. *European Journal of Medicinal Chemistry* **2018**, *144*, 444–492. https://doi.org/10.1016/j.ejmech.2017.12.044.

(28) Adrion, D. Calculating Photochemical Reaction Mechanisms with Multiconfigurational Calculations and Dynamics, Northeastern University, 2023. https://doi.org/10.17760/D20621549.

(29) Uno, B.; Matsuhisa, Y.; Kano, K.; Kubota, T. New Description of the Substituent Effect on Electronic Spectra by Means of Substituent Constants. II. n-π and π-π Transitions. *Chemical & Pharmaceutical Bulletin* **1984**, *32* (5), 1691–1698. https://doi.org/10.1248/cpb.32.1691.

(30) Hartley, G. S. The Cis-Form of Azobenzene. *Nature* **1937**, *140* (3537), 281–281. https://doi.org/10.1038/140281a0.

(31) Brown, C. J. A Refinement of the Crystal Structure of Azobenzene. *Acta Cryst* **1966**, *21* (1), 146–152. https://doi.org/10.1107/S0365110X66002445.

7. Acknowledgments

First and foremost, I am deeply grateful to **Almighty God** for His guidance, blessings, and strength, which have helped me complete this research.

I sincerely thank my supervisor, **Prof. Nobuyuki Tamaoki,** for his invaluable support, encouragement, and guidance throughout my Ph.D. journey. I am also grateful to my supporting supervisor, **Prof. Kuniharu Ijiro,** for the opportunity to join the Ph.D. program, his valuable advice and insights, and to **Dr. Hideyuki Mitomo** for his suggestions and guidance. I particularly appreciate the daily discussions and suggestions from **Dr. P. K. Hashim,** which have been crucial in refining my work.

I would also like to thank **Dr. Saugata Sahu, Dr. Kiyonori Takahashi, and Prof. Takayoshi Nakamura** for their assistance with DFT calculations and X-ray crystal analysis, respectively. Their contributions have been of great help in my work.

I appreciate the kindness and support of my colleagues, **Dr. Ammathnadu S. Amrutha, Dr. Jiajun Qi and Ms. Shifa Ahmad**, who made my time in the lab enjoyable. Their encouragement and assistance have meant a lot to me.

I am also grateful to the **Hokkaido University EXEX fellowship**, whose support made my Ph.D. studies possible.

I extend my heartfelt thanks to **Prof. Yasuteru Urano and Dr. Toru Komatsu** from the Laboratory of Chemistry and Biology at The University of Tokyo, who mentored and guided me during my master's studies and my doctoral research. Their invaluable support, encouragement, and expertise

played a crucial role in shaping my academic and research journey. I am deeply grateful to their laboratory for providing me with a strong foundation in research.

I would like to express my sincere gratitude to all my teachers from the **College of Pharmaceutical Sciences, Calicut**, and my **school teachers**, who have shaped my learning and instilled in me the confidence to dream big. Their guidance has been instrumental in my academic journey.

Finally, I would like to thank my **family**—my **husband, parents, uncle Moothapa, parents-in-law, brother, kids, and relatives**—for their unwavering support, prayers, and encouragement.

I would also like to express my sincere gratitude to my dear friend, **Afrah Zahid**, for her constant emotional support and encouragement throughout this journey. Her kindness and motivation have been a great source of strength for me.

I am also thankful to my **friends** for always being there for me.